0.1% Triton X-100 (Sigma) in PBS and immunoblocked with 10% goat serum in 0.2% Triton X-100 PBS. A primary antibody for EGFP (anti-EGFP rabbit serum, ×500; Molecular Probes, diluted by 10% goat serum in 0.2% Triton X-100 PBS) was applied to the sections at 4°C for 12 h followed by washing in 0.2% Triton X-100 PBS 2 times for 5 min each. Next, the sections were incubated in Histofine Simple Stain Rat MAX-PO (Multi) (Nichirei, Tokyo, Japan) at RT for 30 min. After washing them in 0.2% Triton X-100 PBS 2 times for 5 min each, color was developed with DAB (3,3′-diaminobenzidene) solution using DAB substrate kit (Vector Laboratories, Burlingame, CA, USA) at RT for 10 min. Then, the sections were washed in distilled water (DW) on rotator 2 times for 5 min each. The nuclei were stained with Hematoxylin solution (Wako, Osaka, Japan) for 1 min. The sections were dehydrated in a concentration-ascending alcohol series, fixed with xylene and mounted on slides using Mount in Entellan R neu (Merk, Darmstadt, Germany) and viewed under a light microscope (Olympus BX50, Tokyo, Japan).

Surface preparation analyses

Immunofluorescence analyses were performed on whole-mount surface preparations of cochleae from 4 rats that had undergone auditory nerve compression without cell transplantation. Each animal was placed under deep anesthesia and then perfused intracardially with 0.01 M phosphate-buffered saline (PBS) followed by 4% paraformaldehyde in PBS. The temporal bones were then collected and immersed in the same fixative for 4 h at 4°C. After decalcification, cochleae were microdissected for surface preparation. After rinses with PBS, the samples were permeabilized and blocked by 10% goat serum in 0.2% Triton X-100 PBS at RT for 30 min. The samples were then incubated overnight at 4°C with anti-myosin VIIa polyclonal rabbit IgG antibody (×500; purchased from Tama Hasson, University of California, San Diego, CA, USA) to detect hair cells. After washing in 0.2% Triton X-100 PBS 2 times for 5 min, the samples were incubated for 1 h at RT with goat anti-rabbit IgG-Alexa 546 conjugated (×200 dilution; Molecular Probes). After rinsing on PBS, the samples were mounted onto glass slides, coverslipped with Vectashield mounting medium (Vector Laboratories), and viewed with a confocal laser-scanning microscope (TCS-SP2 Leica Microsystems, Tokyo, Japan).

Results

Compression of the internal meatal portion of auditory nerve causes loss of spiral ganglion neurons with hair cells spared

In the rats that were killed 4 weeks after compression without transplantation, the BAEPs profoundly deteriorated, with loss of all peaks (Fig. 2A). Histological examination of the temporal bones of these rats revealed profound atrophy of the auditory nerve and spiral ganglion cells in each RC (Fig. 2B). In contrast, it was noted that surface preparation studies revealed the preservation of hair cells. In the basal (the region of 80–100% from the apex) and the middle (the region of 50–70% from the

apex) cochlear turns, the number and configuration of hair cells were normal or near-normal, although some disturbances were observed in the apical area (the region of 10–30% from the apex) (Fig. 2C)).

Cells transplanted at the IAM portions of atrophic auditory nerves extensively migrate (group 1) (Figs. 3–5)

In rats (group 1) that had undergone auditory nerve compression followed by transplantation of ES-SDIA cells at the IAM portion of the auditory nerve, we found ES-SDIA cells at a total of 32 locations (10 different sites, including the transplantation site) (Figs. 3A, B). We found transplanted cells at the transplantation site in 4 of these 9 rats and at the fundus of the internal auditory canal (IAC) in 5 of the 9 rats (Fig. 3B). In one rat, a substantial number of DAB-positive transplanted cells were found at the fundus of the IAC 32 days after transplantation (Figs. 4A-a, b). Most of the cells at the fundus were round, although some appeared to have short projections (Fig. 4A-b, inset).

Generally, the shape of the transplanted cells varied according to the sites where they were found. In one rat with transplanted cells in various regions of the auditory nerve and cochlea 31 days after transplantation (Figs. 4B-a, b), the transplanted cells in the middle of the auditory nerve trunk were elongated, without processes, and aligned in tandem (Fig. 4B-a, inset). Transplanted cells found at the Schwann–glial junctional zone in this rat had several EGFP-positive neuritic processes extending toward the peripheral myelin portion (Fig. 4B-c).

In one rat, several clumps of DAB-positive cells were found within the endolymphatic space in the scala media (Figs. 5A–C). One of these cell clumps was attached to the habenula perforata (HP) region where auditory nerve fibers emerge from RC into the scala media (Fig. 5C). In this rat, transplanted cells were found in the bony canal (tractus spiralis foraminosus) connecting the modiolus and RC (Fig. 5D). The transplanted cells were observed in the scala media in 3 of the 9 rats tested in this group (Figs. 3, 5).

In 8 of the 9 rats examined, a few transplanted cells were found in the perilymphatic space (Figs. 3, 4B-b).

Transplantation of cells into atrophic auditory nerve trunk, an efficient way to deliver cells into Rosenthal's canal (group 2)

In 2 of the 3 rats that had undergone auditory nerve compression and then transplantation of ES-SDIA cells into the auditory nerve trunk, most transplanted cells were retained within the nerve trunk (Figs. 6A, B). In one of these rats, the transplanted cells appeared as a relatively large cell mass within the auditory nerve trunk 32 days after transplantation (Fig. 6A-a). Confocal microscopy revealed that neurites extended distally from the cell mass, between the Schwann cells (Figs. 6A-b, c, d). In this rat, we found a substantial number of the transplanted cells within RC (Figs. 6A-e, f) and several cell clumps in the scala tympani (Fig. 6A-a). In another rat in this group, a cluster of the ES-SDIA cells was seen within the auditory nerve trunk 35 days after transplantation (Fig. 6B-a), with long neuritic
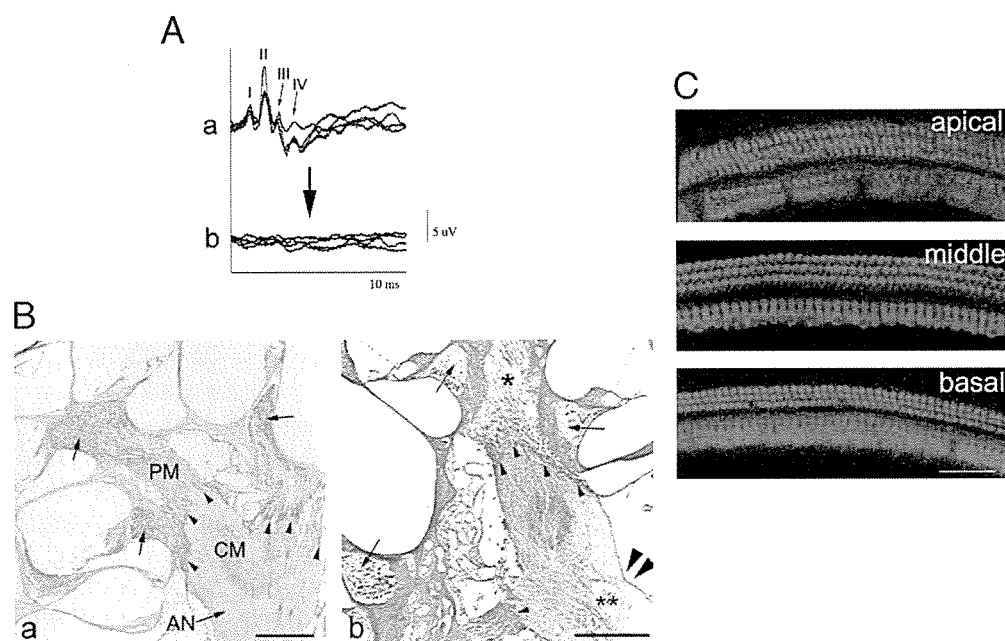
Fig. 2. Auditory nerve degeneration after auditory nerve compression with hair cell spared. (A) Brainstem auditory evoked potentials (BAEPs) before compression (a) and 4 weeks after compression (b). Following compression, all peaks of waves I to IV present before compression (in a) disappeared. (B) Light-microscopic view of the auditory nerve and cochlea in sections from a control (a) and an experimental rat 4 weeks after compression of the auditory nerve (b). Rosenthal's canal in the control rat is densely packed with spiral ganglion cells (arrows in a), but, 4 weeks after compression, the number of spiral ganglion cells in RC of the experimental rat had decreased remarkably (arrows in b) and multiple cavitations were seen (** in b) at the compressed site of the auditory nerve (double arrow heads). A decrease in auditory nerve fibers in the modiolus was seen after compression (* in b). The dome-shaped Schwann–glial junctional zone (SGJ) is indicated by arrow heads. This dome-shaped SGJ is also observed in Figs. 4B and 7. AN, auditory nerve; CM, central myelin portion of the auditory nerve; PM, peripheral myelin portion of the auditory nerve. Hematoxylin–eosin staining. Scale bars, 200 μm. (C) Confocal microscopic views of surface preparations of the cochlea showing the preservation of hair cells. In the basal (the region of 80–100% from the apex) and the middle (the region of 50–70% from the apex) cochlear turns, the number and configuration of hair cells were normal or near-normal. Some disturbances were observed in the apical area (the region of 10–30% from the apex). Scale bars, 50 μm.

processes extending into RC through the bony canals connecting the modiolus and RC (tractus spiralis foraminosus) (Fig. 6B-b).

Cells transplanted to an intact auditory nerve do not migrate

When the same volume of ES-SDIA cells was placed at the IAM portion of an intact auditory nerve, after incision of the connective tissue capsule of the auditory nerve trunk, the results were different from those seen when cells were transplanted to the same location adjacent to an atrophic auditory nerve. In one rat in this group, transplanted cells at the site of transplantation had remarkably extended neurites into the auditory nerve trunk both rostrally and caudally by 32 days after transplantation (Figs. 7A–F), a finding not observed in the rats in group 1 (with atrophic nerves). One neurite that had extended into the peripheral myelin portion of the intact auditory nerve was quite long, and its tip had the shape of a growth cone (Fig. 7B). Although several EGFP-positive cell bodies were observed within the auditory nerve trunk (Fig. 7F), we did not find any transplanted cell bodies very far distant from the site of transplantation.

Discussion

We have demonstrated a technique for cell transplantation to the inner ear that does not involve damage to the membranes that seal the endolymphatic and perilymphatic chambers. Maintenance of the integrity of these chambers is crucial to the auditory system and will significantly reduce the effects of surgical trauma. The technique may have clinical benefits in the future, but it also provides a more controlled model for analysis of the potential for cell transplantation into the inner ear.

We have also demonstrated for the first time that transplanted ES cells can migrate along an atrophic auditory nerve to the scala media where the hair cells reside. The extent of cell migration was related to the compression injury imposed on the auditory nerve. We have yet to demonstrate functional integration of transplanted cells, a challenge that will require further experimentation with a range of different types and preparations of donor cells.

Transplanted cells are transferred to the scala media through atrophic auditory nerve

Successful cell transplantation will depend on how easily transplanted cells can access different parts of the inner ear. The injection site is critical in terms of minimizing tissue damage while placing cells as close as possible to their target site. The migratory behavior of injected cells will determine their ability to locate and replace the target cell populations. The present finding that transplanted cells can travel from the initial grafted site at the IAM portion of the auditory nerve to the most distal end of the auditory nervous system, the scala media where the hair cells reside, suggests a potential delivery route with minimal surgical invasion.
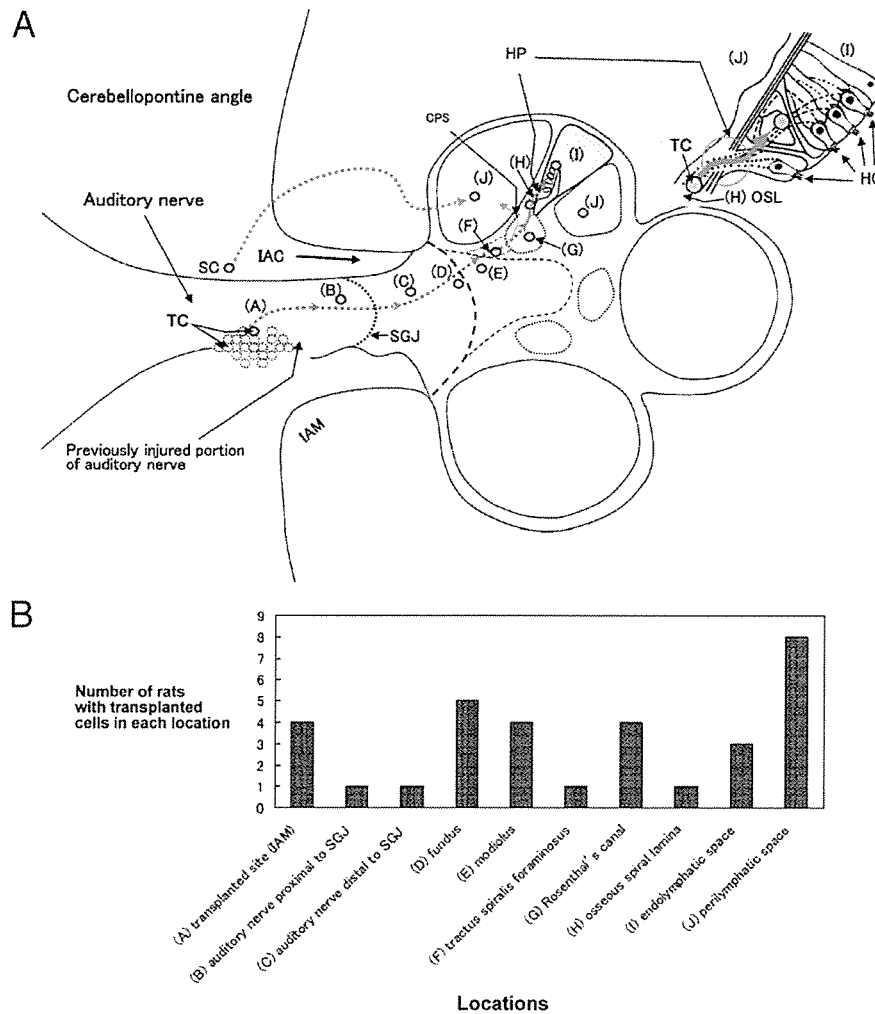
Fig. 3. Cell distribution after transplantation in group 1. (A) Schematic map of the distribution of ES-SDIA cells transplanted at the IAM portion of the auditory nerve (A) in a total of 9 rats. By 4 to 5 weeks after transplantation, the transplanted cells (TC) were found in a total of 32 locations (10 different sites, shown by orange circles) in the 9 rats. The 10 different sites included the transplantation site (A); the auditory nerve proximal (B) and distal (C) to the Schwann–glial junctional zone (SGJ); the fundus of the internal auditory canal (IAC) (D); the modiolus (E); the tractus spiralis foraminosus (F); Rosenthal's canal (G); the osseous spiral lamina (H); the endolymphatic space (I); and the perilymphatic space (J). The blue arrow heads and red solid and dotted arrows indicate the probable route by which the transplanted cells migrated. Spilled cells (SC) probably entered the perilymphatic space (J) through the cochlea aqueduct (Fig. 1, CA) (red dotted curved arrow from SC to (J). CPS, canaliculae perforantes of Schuknecht; HP, habenula perforata. Inset: In the right upper corner is a magnified view of the HP region. HC, hair cells; OSL, osseous spiral lamina. (B) Number of rats (ordinate) with transplanted cells in each of the 10 sites in the auditory nerve and cochlea (abscissa). The sites labeled A to J correspond to those with the same labels in A.

Histopathological examinations of human temporal bones invaded by neoplastic cells indicate that the narrow bony canals between the modiolus and RC (tractus spiralis foraminosus, Figs. 3A–F) serve as a barrier for the passage of cells into RC (Hoshino et al., 1972). In the present study, however, transplanted cells were found within the tractus spiralis foraminosus itself (Figs. 3, 5D) and even in the HP region (Figs. 3, 5C). From these findings, it is likely that transplanted cells reached the scala media by migrating through the HP. Normally, auditory nerve fibers are tightly packed and constricted as they pass through the HP and then they spread out to innervate the hair cells (Spoendlin, 1987). Therefore, under normal conditions, there may be limited space at the HP for the passage of transplanted cells. The apparent ease with which cells migrated along the atrophic nerve could be due to

reduced density of the host tissue. Degeneration of the nerve fibers could leave enough space in the HP for transplanted cells to pass through (Fig. 2B-b). The degenerated nerve may produce signals that facilitate cell migration, but we have no evidence for this possibility. In fact, atrophy of the auditory nerve seemed to be required for cell migration because cells transplanted to intact auditory nerves did not migrate so far (Fig. 7). However, space may not be the only influence since undamaged host nerve tissue may restrict migration by direct inhibition or by more effective induction of cell differentiation such as neurite extension. In undamaged nerve tissue, transplanted cells extended numerous neurites into the nerve trunk and remained at the site of transplantation (Figs. 7A, B).

We think it unlikely that the cells we transplanted migrated into the endolymphatic space through the vestibular aqueduct
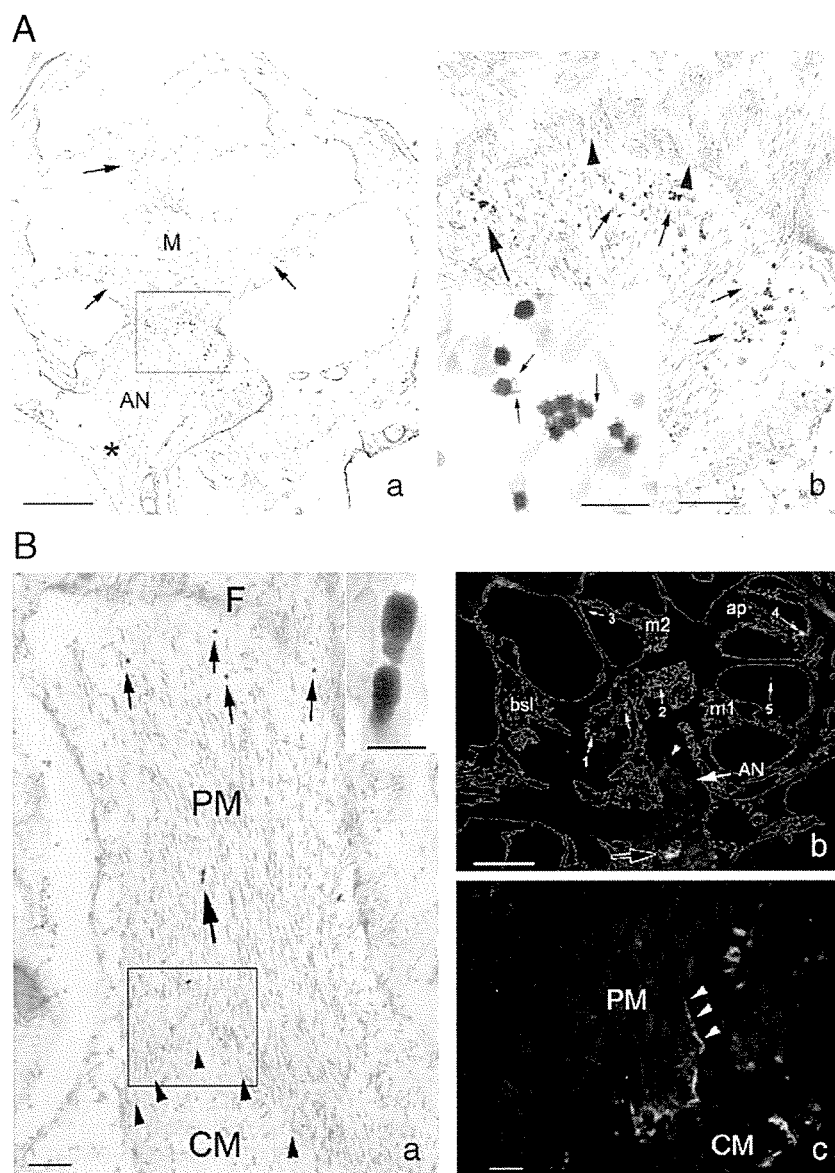
Fig. 4. Migration of ES-SDIA cells transplanted at the IAM portions of atrophic auditory nerves (group 1). (A) Histological appearance of the cochlea showing transplanted ES-SDIA cells accumulated at the fundus of the internal auditory canal in a rat of group 1 (32 days after transplantation). (a) The area of compression and subsequent transplantation of ES-SDIA cells at the auditory nerve (AN) is indicated by the asterisk. The fundus of the internal auditory canal is indicated by the rectangle and enlarged in b. The arrows indicate the Rosenthal's canals. M, modiolus. (b) A substantial number of DAB-positive transplanted cells were found at the fundus (arrows). A group of these cells indicated by the large arrow is enlarged in the inset. In this rat, the transplanted cells were round, and some had short processes projecting from the cell surface (arrows in the inset). The arrow heads indicate the bony holes in the cribriform area that had passed the auditory nerve fibers. Scale bars, 500, 100, and 5; a, b, and inset in b, respectively. (B) Histological appearance of the auditory nerve and cochlea in another rat in group 1 (31 days after transplantation of ES-SDIA cells). (a) DAB-positive transplanted cells (small and large arrows) are present in the auditory nerve trunk. The cells indicated by the large arrow are enlarged in the inset. In this rat, the transplanted cells were elongated, without neuritic processes (inset) and aligned in tandem (compared with findings in A-b). The area indicated by the rectangle is enlarged in c. Arrow heads indicate the dome-shaped Schwann–glial junctional zone. F, fundus of the internal auditory canal. CM and PM, central and peripheral myelin portion of the auditory nerve, respectively. (b) The large black arrow indicates the EGFP-positive cells at the compressed and transplanted portion of the auditory nerve. EGFP-positive cells were observed in various regions such as peri-auditory nerve space (small arrow 1), auditory nerve trunk (2), scala tympani (3), scala media (4), and scala vestibuli (5). An arrow head indicates the area indicated by the rectangle in a. Rosenthal's canal in basal, lower middle, upper middle, and apical cochlear turns are represented by bsl, m1, m2, ap, respectively. (c) At the Schwann–glial junctional zone of this rat, EGFP-positive neuritic process extended toward the peripheral myelin (PM) portion of the auditory nerve (arrow heads). The host auditory nerve stained with DAPI (blue). CM and PM, central and peripheral myelin portion of the auditory nerve, respectively. Scale bars, 500 (5), 20 μm in a (inset), b, c, respectively.

(Fig. 1, [1′]) because the operative site was remote from the aperture of the vestibular aqueduct. In this study, however, transplanted cells were found in the perilymphatic space, mainly in the scala tympani (Figs. 3, 4B-b and 6A-a). It is probable that some transplanted cells entered the cerebrospinal fluid in the CP angle during transplantation and that these cells entered the perilymphatic space through the cochlear aqueduct (Fig. 1, CA). It is also possible that the cells reached the scala tympani by migration from RC through the canaliculae perforantes of Schuknecht (Fig. 3A, CPS). Such coincidental spillage of cells
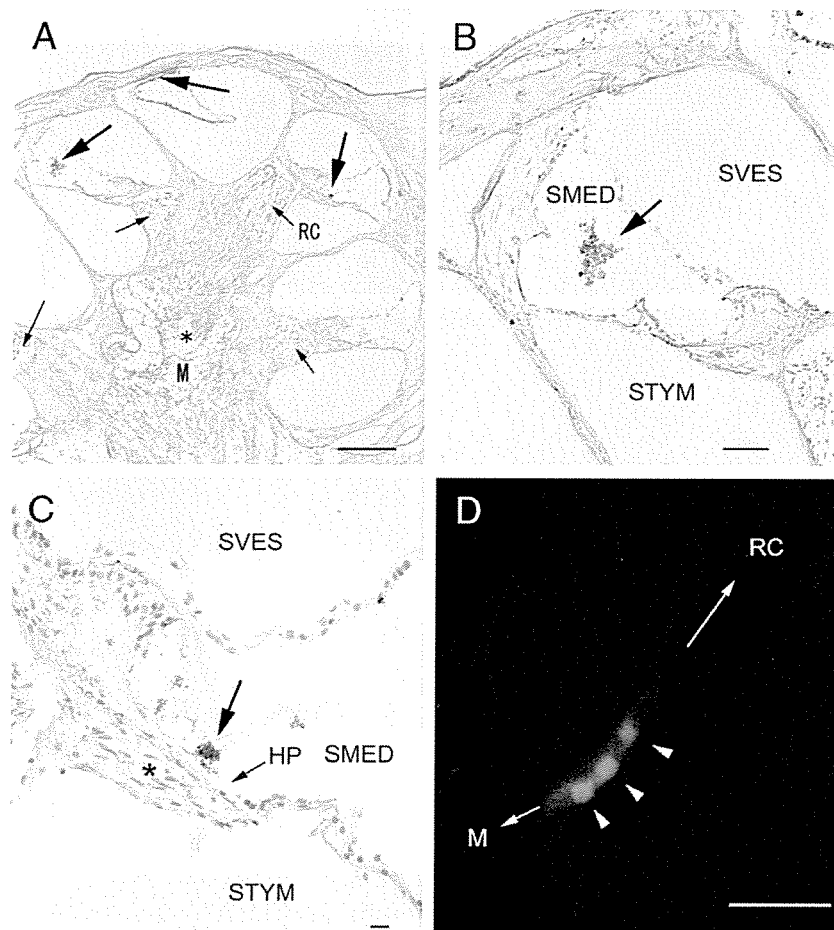
Fig. 5. Migration of ES-SDIA cells transplanted at the IAM portions of atrophic auditory nerves (group 1). (A) Several clumps of DAB-positive cells were found within the endolymphatic space (larger arrows). Two of these cell masses are shown enlarged in B and C. Note empty Rosenthal's canals (RC, small arrows) and paucity of auditory nerve fibers (*) in the modiolus (M). (B) A clump of transplanted cells was found in the scala media (SMED) (arrow). (C) A clump of transplanted cells (arrow) was seen near the habenula perforata (HP) region. Spindle-shaped nuclei of Schwann cells were seen in the osseous spiral lamina (*). (D) EGFP-positive transplanted cells were observed in the bony canal (tractus spiralis foraminosus; arrow heads). The directions to the modiolus and Rosenthal's canal are indicated by M and RC, respectively. Scale bars, 200, 50, 20, and 20 μm in A, B, C, and D, respectively.

may be prevented with future refinements in technique. We found no evidence for substantial accumulation or proliferation of transplanted cells in the perilymphatic space. However, we must be cautious when positioning materials in spaces that communicate with the cerebrospinal fluid space in order to avoid unwanted effects of transplanted materials at inappropriate locations such as the contralateral intact ear.

Local environmental cues and cells with potential for region-specific differentiation

The ES cells we used in this particular study showed a robust migratory ability in the atrophic auditory nerve and were observed at the entire regions of the peripheral auditory nervous system. Ideally, however, the transplanted cells should halt their migration at the target site and then differentiate into region-specific mature cells, for example, spiral ganglion neurons or hair cells. Successful differentiation is likely to depend on local environmental cues and on the capacity of transplanted cells to receive and respond to those cues. In the present study, cells transplanted into the normal auditory nerve extended neuritic processes and

expressed βIII-tubulin (Figs. 7B, C, D, F), but their migration was more restricted. This indicates contextual responses to environmental cues and suggests that some degree of morphological integration of the transplanted cells actually occurred. The normal adult tissue could present cues to induce neurite extensions, and it may even restrict unwanted migration, which could be crucial therapeutically. For example, residual nerves in patients with hearing loss could well be essential for attracting transplanted cells into Rosenthal's canal and inducing their differentiation. In the present study, we induced nearly total loss of SGNs in a relatively acute manner (Fig. 2B-b). However, in our experimental model, by regulating the experimental conditions of auditory nerve compression, we can reproduce a similar situation as observed clinically where fewer SGNs gradually degenerate.

The finding that the transplanted cells assumed various shapes according to the sites where they were found implied that they had been influenced by local environmental cues (Fricker et al., 1999; LaBarge and Blau, 2002). The cells at the fundus were round in shape with cell processes (Fig. 4A-b), but those within the nerve tissue assumed a streamlined shape, without cell processes (Fig. 4B-a). An interesting finding of our study
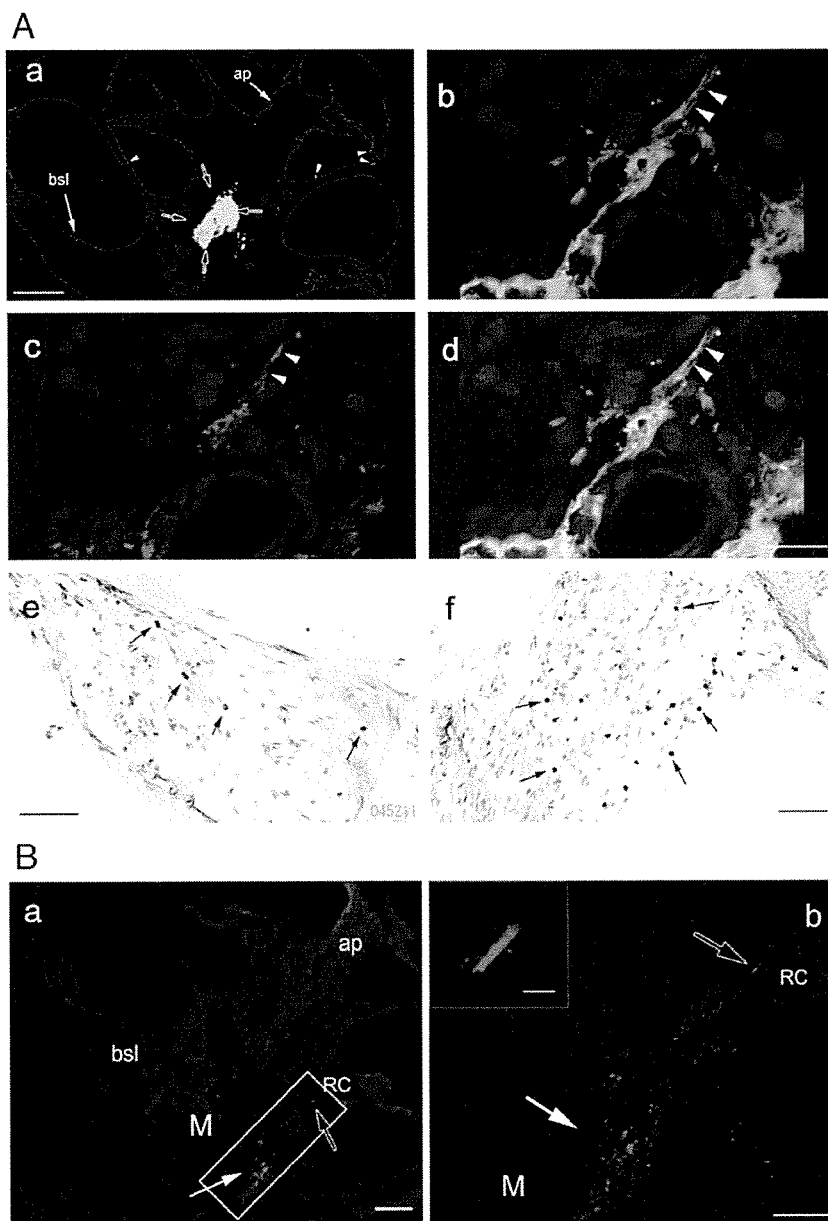
Fig. 6. ES-SDIA cells transplanted into atrophic auditory nerve trunk. (A) Histological appearance of the auditory nerve and cochlea showing transplanted ES-SDIA cells in a rat of group 2 (32 days following transplantation). (a) A relatively large cell mass was found in auditory nerve trunk (arrows). Arrow heads indicate the transplanted cells found in the scala tympani. bsl and ap, basal and apical cochlear turns, respectively. Confocal microscopy revealed an EGFP and βIII-tubulin-positive neurite process (arrow heads) among Schwann cells in b and c, respectively. These images are merged in (d) (arrow heads). The nuclei of the host tissue were stained with TOTO3. The arrows in e and f indicate DAB-positive transplanted cells in the basal and apical turns of the cochlea, respectively. Scale bars, 200, 20, 20, 20, 50, and 50 μm in a, b, c, d, e, and f, respectively. (B) Histological appearance of the auditory nerve and cochlea showing transplanted ES-SDIA cells in a rat of group 2 (35 days after transplantation). (a) A group of transplanted cells (red) was seen in the modiolus (M) (white arrow), and a neuritic process was seen in Rosenthal's canal (RC) (black arrow). Host tissue was stained blue with DAPI. bsl, basal turn; ap, apical turn. The rectangular area is enlarged in b. M, modiolus. (b) Transplanted cells (red) were found within the modiolus (M) (white arrow). A neuritic process that emerged from the bony canal (tractus spiralis foraminosus) and extended into Rosenthal's canal appeared in tangential section (black arrow). Inset: Higher magnification view of neuritic processes indicated by black arrow in b. Compare with the inset in Fig. 7B. Scale bars, 200 and 100 (20) μm in a and b, respectively.

was the remarkable ability of ES-SDIA cells to extend neuritic processes along the auditory nerve (Figs. 4B-c, 6A-b, c, d, 6B and 7). Some transplanted cells with cell bodies in the modiolus had neuritic process extending to RC (Fig. 6B-b), and cells that had migrated to the Schwann–glial junctional zone had neuritic process extending to the peripheral myelin region (Fig. 4B-c). A study that investigated regeneration of axons in the rat optic nerve revealed that axons failed to regenerate in the astrocytic environment (central myelin portion) but readily re-grew in the presence of Schwann cells (peripheral myelin portion), even across the Schwann–glial junctional zone, indicating that resident Schwann cells may exert trophic effects (Berry et al., 1992). This possibility was supported by the findings in the study we report here.

The survival rates of various cells transplanted into the inner ear spaces have been reported to be quite low and no more than
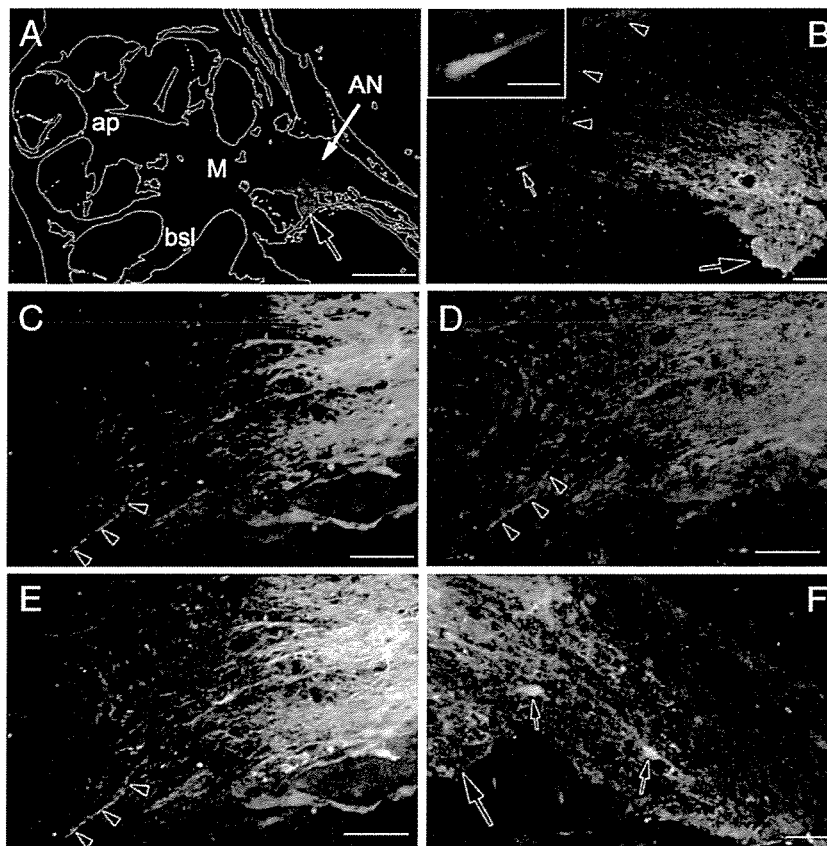
Fig. 7. Histological appearance of the auditory nerve and cochlea showing ES-SDIA cells that had been transplanted to an intact auditory nerve (AN). (A) An EGFP-positive cell mass (black arrow) was seen at the transplantation site in the auditory nerve. bsl, basal turn; ap, apical turn; M, modiolus. (B) Transplanted cell mass (larger arrow) extended neurites distally, and one neurite was found to have extended into the peripheral myelin portion of the auditory nerve trunk (smaller arrow, shown enlarged in the inset). The tip of the neurite had the shape of a growth cone (inset; compare with Fig. 6B-b). Arrow heads indicate the dome-shaped Schwann–glial junctional zone. (C, D) Neurite extensions stained with anti-EGFP (C) and βIII-tubulin (D) staining. One neurite extended into quite a distance into the peripheral myelin portion (arrow heads). (E) Merged view. (F) Neurite extensions and a few cell bodies were also found proximal to the cell transplantation site (smaller black arrows), and a cell mass (larger arrow) was seen attached to the auditory nerve. Host cells stained blue with DAPI in B, C, D, E and F. Scale bars, 500, 50 (20), 100, 100, 100, and 50 μm in A, B (inset), C, D, E, and F, respectively.

2.0% (Hu et al., 2004a,b). It is difficult to make an accurate estimate of survival of transplanted cells. However, the survival rate seems to vary according to the method; intra-neurally transplanted cells (Fig. 6A) seemed to survive more than peri-neurally transplanted cells (Figs. 4, 5). In future studies, we should select appropriate cells with or without some adjunct therapies such as pre-conditioning with neurotrophic factors. It might be beneficial to add some neurotrophic factors such as NGF to foster neurite outgrowth from the cells transplanted to the injured auditory nerve (Hu et al., 2005).

In xenograft transplantation, some immunosuppressant may be beneficial to secure the transplanted cells at the host, although, in the present study, we did not apply this strategy. Refinement of the delivery technique to maximize the survival of transplanted cells and to enhance neuronal differentiation will be investigated in our future studies.

Selective ablation of the auditory neurons with hair cells spared

We found that the hair cells did not degenerate within 4 weeks of damage to the auditory neurons (Figs. 2B, C). Our previous study indicated that the auditory neurons from the apical cochlear turn were injured more than those from more basal cochlear turns in our experimental model (Sekiya et al., 2000). This might have been one of the reasons why some limited signs of hair cell loss were observed in the apical region. In future studies, we could selectively ablate groups of auditory neurons by applying a weaker compression force than used in the present study. Compression injury is precise and does not involve the more widespread and non-specific effects that may occur with pharmacologic methods (Lang et al., 2005; Schmiedt et al., 2002). Taken together, this model may provide unique opportunities to investigate the regeneration of spiral ganglion neurons without being confounded by the changes occurred in the hair cell region.

Candidate materials for cell transplantation therapy to rebuild lost hearing

One reason why we used ES-SDIA cells in this particular study was that they had been induced in advance to differentiate into neural cells versus endo- or mesodermal cells. Other cells, however, could be candidates for transplantation to rebuild lost hearing (Fuchs and Segre, 2000; Morest and Cotanche, 2004).

For example, tissue-specific stem cells derived from inner ear tissue (Bermingham-McDonogh and Rubel, 2003; Germiller et al., 2004; Kalinec et al., 1999; Kojima et al., 2004; Lawoko-Kerali et al., 2004; Li et al., 2003; Nicholl et al., 2005; Rask-Andersen et al., 2005; Rivolta and Holley, 2002) would be expected to have a high possibility of being morphologically and functionally integrated into a host's inner ear.

To avoid problems with tissue rejection, autologous cells such as bone marrow stromal cells could be useful (Munoz-Elias et al., 2004; Ohta et al., 2004). A second possibility is to transplant cells, such as those carrying potentially beneficial genes (such as genes promoting hair cell regeneration or secreting neurotrophins that would enhance the function of existing cells). It would not be necessary for such transplanted cells to be morphologically integrated into the host tissue. Rather, it might be sufficient for them to "float" in the target area such as the endolymphatic space. A third possibility is to deliver neurotrophins, growth factors, or pharmacological agents by placing these materials at the IAM portion of the auditory nerve using drug delivery systems.

Our technique is clinically feasible

Clinically, we can enter into the CP angle using retromastoid craniectomy through an incision behind the ear and place various materials at the IAM portion of the auditory nerve in human. This approach is currently used clinically in a variety of procedures, such as microvascular decompression to treat hemifacial spasm, trigeminal neuralgia, and resection of tumors in the CP angle, including vestibular schwannomas (McLaughlin et al., 1999; Ojemann, 2001; Samii and Matthies, 1997; Sanna et al., 2004). In contrast to the cochlea in small experimental animals such as rat, mouse, and guinea pig, where the cochlear wall is directly sighted in the tympanic bulla, the human cochlea is embedded deep in the temporal bone. Therefore, in order to reach the cochlea wall in humans, the thick bone around the cochlea should be removed without damaging intracochlear structures. This seemed to be quite a difficult task to be performed in comparison with the technique through the CP angle in our technique. Other advantages of our technique include its versatility. For example, when transplantation of cells into the cochlear nucleus region is planned (Hu et al., 2004a), cells can be placed in this region under direct visual control. In contrast to an extensive migration of the transplanted cells towards the regions distal to the transplanted site in this study, we found a very few cells centrally. It is not clear why relatively few cells migrated into the brainstem regions.

We believe that through collaboration and use of techniques such as those reported here, experts in molecular cell engineering, neuro-otology, and neurosurgery will be able to offer hope to many patients with profound hearing disturbances.

References

Bermingham-McDonogh, O., Rubel, E.W., 2003. Hair cell regeneration: winging our way towards a sound future. Curr. Opin. Neurobiol. 13, 119–126.

Berry, M., Hall, S., Rees, L., Carlile, J., Wyse, J.P., 1992. Regeneration of axons in the optic nerve of the adult Browman–Wyse (BW) mutant rat. J. Neurocytol. 21, 426–448.

Bianchi, L.M., Raz, Y., 2004. Methods for providing therapeutic agents to treat damaged spiral ganglion neurons. Curr. Drug Targets. CNS Neurol. Disord. 3, 195–199.

Brown, J.N., Miller, J.M., Altschuler, R.A., Nuttall, A.L., 1993. Osmotic pump implant for chronic infusion of drugs into the inner ear. Hear. Res. 70, 167–172.

Fricker, R.A., Carpenter, M.K., Winkler, C., Greco, C., Gates, M.A., Bjorklund, A., 1999. Site-specific migration and neuronal differentiation of human neural progenitor cells after transplantation in the adult rat brain. J. Neurosci. 19, 5990–6005.

Fuchs, E., Segre, J.A., 2000. Stem cells: a new lease on life. Cell 100, 143–155.

Germiller, J.A., Smiley, E.C., Ellis, A.D., Hoff, J.S., Deshmukh, I., Allen, S.J., Barald, K.F., 2004. Molecular characterization of conditionally immortalized cell lines derived from mouse early embryonic inner ear. Dev. Dyn. 231, 815–827.

Holley, M.C., 2002. Application of new biological approaches to stimulate sensory repair and protection. Br. Med. Bull. 63, 157–169.

Hoshino, T., Hiraide, F., Nomura, Y., 1972. Metastatic tumour of the inner ear: a histopathological report. J. Laryngol. Otol. 86, 697–707.

Hu, Z., Ulfendahl, M., Olivius, N.P., 2004a. Central migration of neuronal tissue and embryonic stem cells following transplantation along the adult auditory nerve. Brain Res. 1026, 68–73.

Hu, Z., Ulfendahl, M., Olivius, N.P., 2004b. Survival of neuronal tissue following xenograft implantation into the adult rat inner ear. Exp. Neurol. 185, 7–14.

Hu, Z., Ulfendahl, M., Olivius, N.P., 2005. NGF stimulates extensive neurite outgrowth from implanted dorsal root ganglion neurons following transplantation into the adult rat inner ear. Neurobiol. Dis. 18, 184–192.

Ito, J., Kojima, K., Kawaguchi, S., 2001. Survival of neural stem cells in the cochlea. Acta Oto-Laryngol. 121, 140–142.

Izumikawa, M., Minoda, R., Kawamoto, K., Abrashkin, K.A., Swiderski, D.L., Dolan, D.F., Brough, D.E., Raphael, Y., 2005. Auditory hair cell replacement and hearing improvement by Atoh1 gene therapy in deaf mammals. Nat. Med. 11, 271–276.

Kalinec, F., Kalinec, G., Boukhvalova, M., Kachar, B., 1999. Establishment and characterization of conditionally immortalized organ of corti cell lines. Cell Biol. Int. 23, 175–184.

Kawasaki, H., Mizuseki, K., Nishikawa, S., Kaneko, S., Kuwana, Y., Nakanishi, S., Nishikawa, S.I., Sasai, Y., 2000. Induction of midbrain dopaminergic neurons from ES cells by stromal cell-derived inducing activity. Neuron 28, 31–40.

Kojima, K., Tamura, S., Nishida, A.T., Ito, J., 2004. Generation of inner ear hair cell immunophenotypes from neurospheres obtained from fetal rat central nervous system in vitro. Acta Oto-Laryngol. 26–30.

LaBarge, M.A., Blau, H.M., 2002. Biological progression from adult bone marrow to mononucleate muscle stem cell to multinucleate muscle fiber in response to injury. Cell 111, 589–601.

Lang, H., Schulte, B.A., Schmiedt, R.A., 2005. Ouabain induces apoptotic cell death in Type I spiral ganglion neurons, but not type II neurons. J. Assoc. Res. Otolaryngol. 6, 63–74.

Lawoko-Kerali, G., Milo, M., Davies, D., Halsall, A., Helyer, R., Johnson, C. M., Rivolta, M.N., Tones, M.A., Holley, M.C., 2004. Ventral otic cell lines as developmental models of auditory epithelial and neural precursors. Dev. Dyn. 231, 801–814.

Li, H., Liu, H., Heller, S., 2003. Pluripotent stem cells from the adult mouse inner ear. Nat. Med. 9, 1293–1299.

McLaughlin, M.R., Jannetta, P.J., Clyde, B.L., Subach, B.R., Comey, C.H., Resnick, D.K., 1999. Microvascular decompression of cranial nerves: lessons learned after 4400 operations. J. Neurosurg. 90, 1–8.

Minor, L.B., 2003. Labyrinthine fistulae: pathobiology and management. Curr. Opin. Otolaryngol. Head Neck Surg. 11, 340–346.

Morest, D.K., Cotanche, D.A., 2004. Regeneration of the inner ear as a model of neural plasticity. J. Neurosci. Res. 78, 455–460.

Morest, D.K., Kim, J., Bohne, B.A., 1997. Neuronal and transneuronal degeneration of auditory axons in the brainstem after cochlear lesions in the chinchilla: cochleotopic and non-cochleotopic patterns. Hear. Res. 103, 151–168.

Munoz-Elias, G., Marcus, A.J., Coyne, T.M., Woodbury, D., Black, I.B., 2004. Adult bone marrow stromal cells in the embryonic brain: engraftment, migration, differentiation, and long-term survival. J. Neurosci. 24, 4585–4595.

Nicholl, A.J., Kneebone, A., Davies, D., Cacciabue-Rivolta, D.I., Rivolta, M. N., Coffey, P., Holley, M.C., 2005. Differentiation of an auditory neuronal cell line suitable for cell transplantation. Eur. J. Neurosci. 22, 343–353.

Ohta, M., Suzuki, Y., Noda, T., Ejiri, Y., Dezawa, M., Kataoka, K., Chou, H., Ishikawa, N., Matsumoto, N., Iwashita, Y., Mizuta, E., Kuno, S., Ide, C., 2004. Bone marrow stromal cells infused into the cerebrospinal fluid promote functional recovery of the injured rat spinal cord with reduced cavity formation. Exp. Neurol. 187, 266–278.

Ojemann, R.G., 2001. Retrosigmoid approach to acoustic neuroma (vestibular schwannoma). Neurosurgery 48, 553–558.

Pujol, R., Puel, J.L., Gervais d'Aldin, C., Eybalin, M., 1993. Pathophysiology of the glutamatergic synapses in the cochlea. Acta Oto-Laryngol. 113, 330–334.

Rask-Andersen, H., Bostrom, M., Gerdin, B., Kinnefors, A., Nyberg, G., Engstrand, T., Miller, J.M., Lindholm, D., 2005. Regeneration of human auditory nerve. In vitro/in video demonstration of neural progenitor cells in adult human and guinea pig spiral ganglion. Hear. Res. 203, 180–191.

Regala, C., Duan, M., Zou, J., Salminen, M., Olivius, P., 2005. Xenografted fetal dorsal root ganglion, embryonic stem cell and adult neural stem cell survival following implantation into the adult vestibulocochlear nerve. Exp. Neurol. 193, 326–333.

Rivolta, M.N., Holley, M.C., 2002. Cell lines in inner ear research. J. Neurobiol. 53, 306–318.

Sakamoto, T., Nakagawa, T., Endo, T., Kim, T.S., Iguchi, F., Naito, Y., Sasai, Y., Ito, J., 2004. Fates of mouse embryonic stem cells transplanted into the inner ears of adult mice and embryonic chickens. Acta Oto-Laryngol. 48–52 (Suppl.).

Samii, M., Matthies, C., 1997. Management of 1000 vestibular schwannomas (acoustic neuromas): hearing function in 1000 tumor resections. Neurosurgery 40, 248–260 (discussion 260–242).

Sanna, M., Taibah, A., Russo, A., Falcioni, M., Agarwal, M., 2004. Perioperative complications in acoustic neuroma (vestibular schwannoma) surgery. Otol. Neurotol. 25, 379–386.

Schmiedt, R.A., Okamura, H.O., Lang, H., Schulte, B.A., 2002. Ouabain application to the round window of the gerbil cochlea: a model of auditory neuropathy and apoptosis. J. Assoc. Res. Otolaryngol. 3, 223–233.

Sekiya, T., Hatayama, T., Shimamura, N., Suzuki, S., 2000. An in vivo quantifiable model of cochlear neuronal degeneration induced by central process injury. Exp. Neurol. 161, 490–502.

Sekiya, T., Yagihashi, A., Shimamura, N., Asano, K., Suzuki, S., Matsubara, A., Namba, A., Shinkawa, H., 2003. Apoptosis of auditory neurons following central process injury. Exp. Neurol. 184, 648–658.

Spoendlin, H., 1987. The afferent innervation of the cochlea. In: Naunton, F.R., C (Eds.), Evoked Electrical Activity in the Auditory Nervous System. Academic Press, New York, pp. 21–41.

Staecker, H., Li, D., O'Malley Jr., B.W., Van De Water, T.R., 2001. Gene expression in the mammalian cochlea: a study of multiple vector systems. Acta Otolaryngol. 121, 157–163.

Starr, A., Picton, T.W., Sininger, Y., Hood, L.J., Berlin, C.I., 1996. Auditory neuropathy. Brain 119 (Pt. 3), 741–753.

Yagihashi, A., Sekiya, T., Suzuki, S., 2005. Macrophage colony stimulating factor (M-CSF) protects spiral ganglion neurons following auditory nerve injury: morphological and functional evidence. Exp. Neurol. 192, 167–177.

187

Original Research Report

Molecular Cloning and Function of Oct-3 Isoforms in Cynomolgus Monkey Embryonic Stem Cells

YASUKO FUJIMOTO,[1–3] KOUICHI HASEGAWA,[1,2] HIROFUMI SUEMORI,[1] JUICHI ITO,[3] and NORIO NAKATSUJI[2]

ABSTRACT

Oct-3 is a key molecule for maintaining self-renewal in mouse embryonic stem (ES) cells. The function of Oct-3 in ES cells of other species, however, especially primate ES cells, is not clear. In the present study, we cloned two splicing isoforms of Oct-3, Oct-3A and Oct-3B, from cynomolgus monkey ES cells, and found that they have high homology to human Oct-3A and Oct-3B. To examine their function, Oct-3A and Oct-3B were overexpressed in cynomolgus monkey ES cells. Transient Oct-3A overexpression induced ES cell differentiation into endodermal and mesodermal lineages and disrupted proliferation of undifferentiated monkey ES cells. In contrast, Oct-3B overexpression did not induce differentiation of monkey ES cells. These findings indicate that a certain Oct-3A expression level has an important role in sustaining self-renewal in non-human primate ES cells.

INTRODUCTION

EMBRYONIC STEM (ES) CELLS are derived from the inner cell mass (ICM) of preimplantation embryos (1). Mouse ES cell lines, which were first established in 1981 by Evans and Kaufman (1), have the capacity to differentiate into all cell types derived from the three primary germ layers, and are capable of long-term renewal in vitro (2). Non-human primate ES cell lines were established from rhesus monkey in 1995 (3), common marmoset in 1996 (4), and cynomolgus monkey in 2001 (5). Human ES cell lines were established in 1998 (6). Human ES cells are expected to be powerful and promising tools for regenerative medicine, and non-human primate ES cells, which are more closely related to human ES cells than rodent ES cells, are expected to be valuable preclinical models. Most research, however, has been limited to ap-

plication in rodent models. Studies in which primate ES cells have been applied to primate disease models are limited (7). Verifying the effects and safety of new methods in non-human primates is an indispensable intermediary step for regenerative medicine before applying new therapeutic strategies to humans.

Although previous research indicates that primate ES cells have a differentiation potency similar to that of mouse ES cells, there are several differences between primate and mouse ES cells. For example, the role of the signaling pathways in ES cell self-renewal, such as the LIF/JAK/Stat3 pathway (8–11) and the BMP/ Id pathway, differs between mouse and primate ES cells (12–14). It is, therefore, important to clarify the mechanisms through which self-renewal of primate ES cells is stably maintained to apply it to large-scale preclinical research.

[1]Laboratory of Embryonic Stem Cell Research, Stem Cell Research Center, [2]Department of Development and Differentiation, Institute for Frontier Medical Sciences, Kyoto University, 606-8507, Japan.
[3]Department of Otolaryngology, Head and Neck Surgery, Graduate School of Medicine, Kyoto University, Kyoto, 606-8507, Japan.

566

The POU transcription factor Oct-3 (also known as Oct-4, Oct-3/4, encoded by *POU5F1*) (15–17) functions as a key molecule in maintaining pluripotency and germline development in mammals (18,19). Oct-3 is expressed in totipotent and pluripotent cells in oocytes and pregastrulation embryos, and it is also highly expressed in ES, embryonic carcinoma, and embryonic germ cell lines (20–24). In mouse ES cells, a certain amount of Oct-3 is critical for maintaining ES cell self-renewal, and any up- or down-regulation induces various cell fates. Using a tetracycline-regulated Oct-3 expression system, Niwa and colleagues showed that decreasing Oct-3 expression to less than half in mouse ES cells drives formation of trophectoderm lineage cells, and increasing Oct-3 expression by more than half increases differentiation into primitive endoderm and mesoderm lineage cells (19).

In humans, there are two splicing isoforms of Oct-3 mRNA, Oct-3A and Oct-3B (25), that have not been reported in mouse. Oct-3A is considered to be the human ortholog of mouse Oct-3, and shares 87% amino acid identity with mouse Oct-3 (25). Oct-3B is a minor splicing variant form of Oct-3A mRNA. Oct-3A and Oct-3B comprise 360 and 265 amino acids, respectively, and share a 225-amino-acid sequence at their carboxy-terminal region, including the POU-specific and POU homeodomains. Oct-3B lacks the proline-rich region of Oct-3A at its amino-terminal region, which is reported to have transcriptional activity in mouse ES cells (26,27).

There have only been a few studies of Oct-3B. Takeda et al. first reported that Oct-3B mRNA was expressed in adult human tissues at low levels, but some of the population would be assumed to have no Oct-3B expression because of polymorphisms in the *POU5F1* codon (25). Caufmann et al. reported that Oct-3B in human blastocysts is localized in the cytoplasm rather than in the nucleus, whereas Oct-3A is highly concentrated in the nucleus (28). Both authors presumed a functional difference between the Oct-3 isoforms in humans, but there have been no reports on the expression of the Oct-3 isoform or the functional difference between Oct-3A and Oct-3B in primate ES cells, including human ES cells.

The function of Oct-3 in primate ES cells is far from fully understood compared with that in mouse ES cells. There have been two reported Oct-3 knockdown experiments in human ES cells, both of which resulted in cell differentiation into the endoderm lineage (29,30). One of these studies reported cell differentiation into the trophectoderm lineage (30), whereas the other did not (29). These studies were performed using small interference (si) RNA that worked on both Oct-3A and Oct-3B, and thus were not capable of distinguishing between the functions of the isoforms. Furthermore, overexpression experiments of each isoform have not been performed, although they are indispensable for fully understanding Oct-3 function in the self renewal of primate ES cells.

In this report, we cloned Oct-3 isoforms in cynomolgus monkey ES cells and quantified the expression of each protein by western blotting. In monkey, as in humans, there are two Oct-3 isoforms; thus, monkey ES cells are a good model of human ES cells. We demonstrated that Oct-3A overexpression in cynomolgus ES cells induced differentiation toward endodermal and mesodermal lineages, whereas that of Oct-3B did not.

MATERIALS AND METHODS

Cell culture

A cynomolgus monkey ES cell line, CMK6, was cultured as previously described (5). Briefly, the cells were maintained on a feeder layer of mouse embryonic fibroblasts (MEFs) treated with mitomycin C in Dulbecco's modified Eagle's medium/Nutrient Mixture F12 Ham (DMEM/F12) (Sigma Aldrich, St. Louis, MO) supplemented with 20% knockout serum replacement (KSR) (Invitrogen, Carlsbad, CA), 0.1 mM 2-mercaptoethanol, 1 mM minimal essential medium (MEM) nonessential amino acids, 2 mM L-glutamine, and 1 mM sodium pyruvate.

Mouse R1 ES cells (31) were cultured on MEFs in DMEM/F12 supplemented with 15% fetal bovine serum (FBS; HyClone, Boston, MA), 0.1 mM 2-mercaptoethanol, 2 mM L-glutamine, 1 mM sodium pyruvate, 1 mM MEM nonessential amino acids, and 1,000 U/ml recombinant mouse leukemia inhibitory factor (LIF) (Chemicon International, Temecula, CA).

Cloning of monkey Oct-3 cDNA

The specific primers for the open reading frames (ORFs) of human Oct-3A and Oct-3B had the following sequences. Oct-3A-specific forward primer, 5′-ATG-GCGGGACACCTGGCTTC -3′; Oct-3B-specific forward primer, 5′-AGGCAGATGCACTTCTACAGAC-3′; common reverse primer for the Oct-3 isoforms, 5′-AGGCAGGCACCTCAGTTTGAATG-3′.

Using these primers, the ORFs of monkey Oct-3 were amplified by reverse transcription (RT) PCR with mRNA from CMK6 ES cells. The PCR products were ligated into a pGEM-T easy vector (Promega, Madison, WI), and these sequences were confirmed by nucleotide sequence analysis.

Plasmid construction

Oct-3A and Oct-3B overexpression vectors, driven by a CAG promoter, which is a strong promoter in mammals (32), were created by inserting the Oct-3A and Oct-3B ORFs into pCAG/PGKneo vectors (10). pCAG/PGK-

567

189

neo vectors without an Oct-3 component were used as mock transfection vectors (Mock).

Introduction of expression vectors into monkey and mouse ES cells

To establish stable transfected cynomolgus monkey ES clones, transfection to cynomolgus ES cells was performed as follows. On 60-mm feeder dishes, 2.4×10^5 CMK6 cells were plated 16 h prior to transfection and were transfected for 2 h with Opti-MEM (Invitrogen) containing linearized plasmid DNA in complex with 20 μl of Lipofectamine 2000 (Invitrogen). To ensure introduction of an equal number of vector molecules, 10 μg of Oct-3A or Oct-3B expression vectors, and 8 μg of Mock vector were used for each transfection. After selection in the presence of 100 μg/ml G418 (Sigma Aldrich) for 10 days, resistant colonies were counted or recovered and plated on new feeder layers.

The mouse R1 ES cells were trypsinized and resuspended in phosphate-buffered saline (PBS), and 1×10^7 cells were electroporated with linearized plasmid DNA at 250 V and 500 μF in a 0.4-cm cuvette using a Gene Pulser (Bio-Rad, Hercules, CA). The amounts of the plasmids were 25 μg each of Oct-3A and Oct-3B expression vectors and 20 μg of Mock vector. Cells were cultured on 100-mm gelatin-coated dishes in the presence of 200 μg/ml G418 for 7 days, and the number of colonies was counted.

Alkaline phosphatase staining

ES cells were fixed with 3.7% formaldehyde in PBS for 20 min at room temperature, and alkaline phosphatase (ALP) activity was detected with Vector Red substrate (Vector Laboratories, Burlingame, CA).

Immunoblot analysis

To remove feeder cells, ES cells were plated on MEF extracellular matrix (ECM)-coated dishes (10). The cells were lysed in 100 μl of lysis buffer containing 50 mM Tris-HCl, pH 7.5, 0.15 M NaCl, 25 mM β-glycerophosphate, 10 mM NaF, 1 mM Na_3VO_4, 1% Triton X-100, 10% glycerol, and the protease inhibitor cocktail, Complete Mini (Roche, Switzerland).

The lysate samples were separated by sodium dodecyl sulfate-polyacrylamide gel electrophoresis (SDS-PAGE), electroblotted onto an Immun-Blot PVDF Membrane (Bio-Rad), and probed with primary antibodies. After incubation with horseradish peroxidase (HRP)-conjugated secondary antibodies (Dako Cytomation, Denmark), proteins reacting with antibodies were detected using enhanced chemiluminescence reagent (Western Blotting Luminol Reagent; Santa Cruz Biotechnology, Santa Cruz, CA), and analyzed by autoradiography. Anti-Oct4 (Oct-3) polyclonal antibodies (AB-3209, Chemicon International) whose epitope is common to Oct-3A and Oct-3B were used to detect both isoforms on the same membrane with different exposure times. The standardization of the samples was performed using anti-β-actin monoclonal (AC-15) antibody (A-5441, Sigma Aldrich). Signal intensity was measured using pixel intensity analysis with Scion Image software (Scion Corporation, http://www.scioncorp.com/).

Formation of embryoid bodies of monkey ES cells

Cynomolgus ES cells were treated with 0.25% trypsin supplemented with 1 mM $CaCl_2$ and 20% KSR (5) and detached from feeder cells by gentle pipetting to avoid dissociation of colonies. The cells were cultured in suspension in petri dishes and aggregated to form embryoid bodies (EBs). EBs were grown in ES medium for 10 days and collected for preparation of total RNA.

Transient transfection and RT-PCR analysis

For transient transfection with the expression vectors, 1.2×10^5 cynomolgus ES cells cultured on a feeder layer in 35-mm dishes were transfected with 5 μg of either Oct-3A or Oct-3B expression plasmid, or alternatively, with 4 μg mock plasmid, in 10 μl of Lipofectamine 2000. They were cultured initially for 2 h, then, after the medium was replaced, samples were collected at 24 and 48 h.

Total RNA was extracted from ES cells or from 10-day-old wild-type EBs using Trizol (Invitrogen), according to the manufacturer's protocol. Total RNA was then treated with DNase I (Takara Biotechnology, Japan), and cDNA was synthesized from 2 μg of total RNA using an RNA PCR kit (AMV) Ver3.0 (Takara Biotechnology).

Ex Taq polymerase (Takara Biotechnology) was used for the PCR reactions, which were then optimized to allow for semiquantitative comparisons within the log phase of amplification. The gene-specific primers, listed in Table 1, were designed based on published human mRNA sequences and did not cross-react with the mouse feeder cells.

RESULTS

Cloning of Oct-3A and Oct-3B from monkey ES cells

To examine whether Oct-3 isoforms exist in monkey ES cells, we performed RT-PCR cloning using variant-specific primers designed from human Oct-3A and Oct-3B cDNA, and obtained two types of cDNA clones. The

568

TABLE 1. PRIMERS USED IN RT-PCR STUDIES

Gene	Primer sequence (5' → 3')	Annealing temperature (°C)	Cycles	Product size (bp)
albumin	for-GCATCCTGATTACTCTGACATG	58°C	32	229
	rev-CTTGGTGTAACGAACTAATTGC			
AFP	for-TCAGTGAGGACAAACTATTGGC	56°C	25	262
	rev-CACCCTGAGCTTGACACAGA			
goosecoid	for-GCTTCTCAACCAGCTGCAC	60°C	33	250
	rev-TGCTGATGATCTTGAGGCT			
Cdx2	for-TCACCATCCGGAGGAAAGCC	65°C	32	670
	rev-AGAGGTGCAGCCTGCAGATC			
NF68kD	for-GGCGCGCTATGAAGAGGAG	55°C	33	422
	rev-CTTGGCCTTGAGCAGACGA			
Oct-3A	for-ATGGCGGGACACCTGGCTTC	65°C	25	1094
	rev-AGGCAGGCACCTCAGTTTGAATG			
Oct-3B	for-AGGCAGATGCACTTCTACAGAC	65°C	25	815
	rev-AGGCAGGCACCTCAGTTTGAATG			
GAPDH	for-ACCAGGGCTGCTTTTAACTC	60°C	22	215
	rev-TTGCTGATGATCTTGAGGCT			

for- and rev- stand for forward primer and reverse primers, respectively.

cDNA amplified with human Oct-3A specific primers was 1,083 bp and the cDNA amplified with human Oct-3B specific primers was 798 bp. These cDNA clones were the same size as the reported ORFs of human Oct-3A and Oct-3B, and had highly homologous nucleic acid sequences (98.2% and 98.6%, respectively) and deduced amino acid sequences (98.6% and 98.5%, respectively) (Fig. 1A,B). These two products were, therefore, considered to be the ORFs of monkey Oct-3A and Oct-3B because they have a common structure in the last 678 bp. Thus, they were considered to be splicing variant isoforms, as reported in humans. Similar to mouse Oct-3 and human Oct-3A, monkey Oct-3A has a proline-rich domain at the amino terminal, which is a transcription activation domain in mouse ES cells (26,27). In contrast, Oct-3B lacks this domain. To confirm the expression of Oct-3A and Oct-3B proteins in monkey ES cells, we performed western blot analysis using anti-Oct-3 antibodies that recognize the carboxyl termini of human Oct-3 shared by both isoforms. Both Oct-3A and Oct-3B were detected in monkey ES cells (Fig. 1C). Protein expression of Oct-3B in monkey ES cells, however, was much lower than that of Oct-3A.
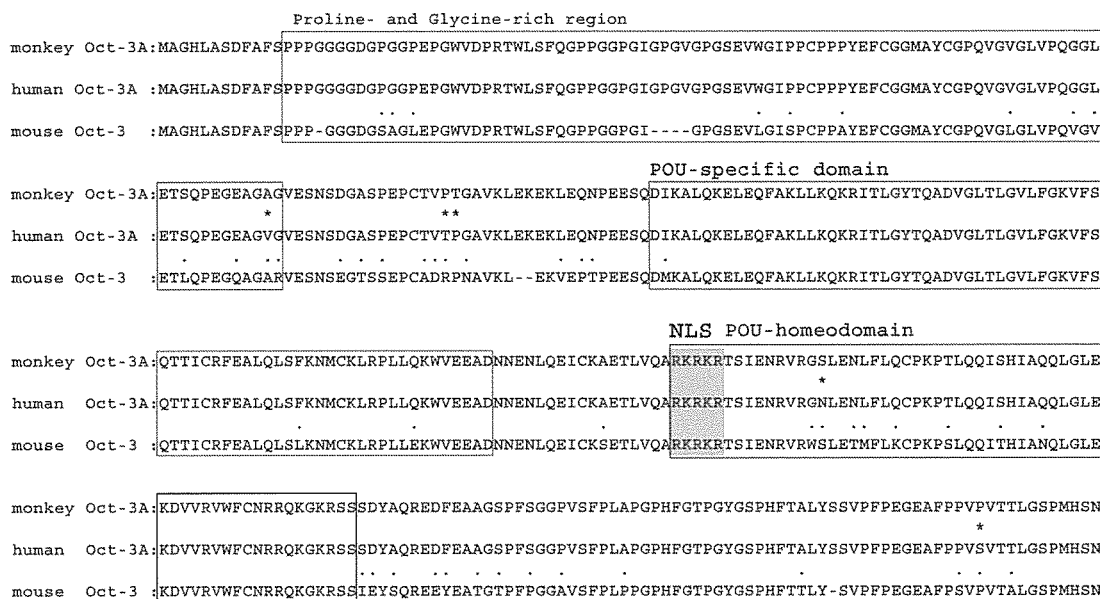
Establishment of stable transfectants of Oct-3A or Oct-3B overexpression vectors

Because up-regulation of Oct-3 by 50% above the normal level promotes differentiation of mouse ES cells into primitive endodermal or mesodermal lineages (19), we constructed and transfected Oct-3A and Oct-3B overex-

pression vectors to examine whether a particular Oct-3 expression range is required for maintaining undifferentiated states in monkey ES cells. We first electroporated these vectors into mouse ES cells to estimate whether the vectors were functional. After 1 week of G418 selection, 75% of the surviving colonies in Oct-3A-transfected mouse ES cells were completely differentiated, whereas only 10% of colonies were completely differentiated in Mock and Oct-3B transfected cells (Fig. 2A,C). This finding suggested that Oct-3 protein produced from the vectors is functional, and that, like mouse Oct-3, overexpression of Oct-3A, but not Oct-3B, affects the self-renewal of mouse ES cells.

Next, we transfected these vectors into cynomolgus monkey ES cells. Unlike the results obtained using mouse ES cells, the ratio of undifferentiated and differentiated colonies in these transfected monkey ES cells was not significantly different among the plasmids, and most of the colonies of each of the transfected cells were undifferentiated (Fig. 2D,G). The total number of surviving colonies in Oct-3A- and Oct-3B-transfected cells, however, was smaller than that in mock-transfected cells (Fig. 2F), and this was also observed in the case of mouse ES cells (Fig. 2B). To examine whether this reduction in colony numbers resulted from differences in plasmid transfection efficiency or differences in the effects of Oct-3A and Oct-3B overexpression, we performed a transfection assay using vectors linearized at the XbaI site. This site is located at the junction of the promoter and either Oct-3A or Oct-3B cDNA to avoid expression of exogenous Oct-3A or Oct-3B from the vectors. There

569

191

A

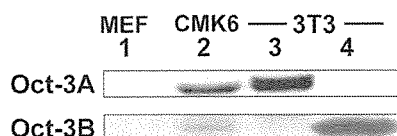Proline- and Glycine-rich region

```
monkey Oct-3A:MAGHLASDFAFSPPPGGGGDGPGGPEPGWVDPRTWLSFQGPPGGPGIGPGVGPGSEVWGIPPCPPPYEFCGGMAYCGPQVGVGLVPQGGL

human  Oct-3A :MAGHLASDFAFSPPPGGGGDGPGGPEPGWVDPRTWLSFQGPPGGPGIGPGVGPGSEVWGIPPCPPPYEFCGGMAYCGPQVGVGLVPQGGL
                            .  .                              .   .       .                        .  .
mouse  Oct-3  :MAGHLASDFAFSPPP-GGGDGSAGLEPGWVDPRTWLSFQGPPGGPGI----GPGSEVLGISPCPPAYEFCGGMAYCGPQVGLGLVPQVGV
```

POU-specific domain

```
monkey Oct-3A:ETSQPEGEAGAGVESNSDGASPEPCTVPTGAVKLEKEKLEQNPEESQDIKALQKELEQFAKLLKQKRITLGYTQADVGLTLGVLFGKVFS
                          *                    **                 Q
human  Oct-3A :ETSQPEGEAGVGVESNSDGASPEPCTVPTGAVKLEKEKLEQNPEESQDIKALQKELEQFAKLLKQKRITLGYTQADVGLTLGVLFGKVFS
                          .       .  .   ... .                     .
mouse  Oct-3  :ETLQPEGQAGARVESNSEGTSSEPCADRPNAVKL--EKVEPTPEESQDMKALQKELEQFAKLLKQKRITLGYTQADVGLTLGVLFGKVFS
```

NLS POU-homeodomain

```
monkey Oct-3A:QTTICRFEALQLSFKNMCKLRPLLQKWVEEADNNENLQEICKAETLVQARKRKRTSIENRVRGSLENLFLQCPKPTLQQISHIAQQLGLE
                                                                              *
human  Oct-3A :QTTICRFEALQLSFKNMCKLRPLLQKWVEEADNNENLQEICKAETLVQARKRKRTSIENRVRGNLENLFLQCPKPTLQQISHIAQQLGLE
                                                                       ..     ..      .
mouse  Oct-3  :QTTICRFEALQLSLKNMCKLRPLLEKWVEEADNNENLQEICKSETLVQARKRKRTSIENRVRWSLETMFLKCPKPSLQQITHIANQLGLE
```

```
monkey Oct-3A:KDVVRVWFCNRRQKGKRSSSDYAQREDFEAAGSPFSGGPVSFPLAPGPHFGTPGYGSPHFTALYSSVPFPEGEAFPPVPVTTLGSPMHSN
                                                                                          *
human  Oct-3A:KDVVRVWFCNRRQKGKRSSSDYAQREDFEAAGSPFSGGPVSFPLAPGPHFGTPGYGSPHFTALYSSVPFPEGEAFPPVSVTTLGSPMHSN
               ..     ..  .    . .                                                  .         ..   .
mouse  Oct-3  :KDVVRVWFCNRRQKGKRSSIEYSQREEYEATGTPFPGGAVSFPLPPGPHFGTPGYGSPHFTTLY-SVPFPEGEAFPSVPVTALGSPMHSN
```

B

POU-specific domain

```
monkey Oct-3B:MHFYRLFLGATRRFLNPEWKGEIDNWCVYVLTSLLPFKIQSQDIKALQKELEQFAKLLKQKRITLGYTQADVGLTLGVLFGKVFSQTTIC

human  Oct-3B:MHFYRLFLGATRRFLNPEWKGEIDNWCVYVLTSLLPFKIQSQDIKALQKELEQFAKLLKQKRITLGYTQADVGLTLGVLFGKVFSQTTIC
```

NLS POU-homeodomain

```
monkey Oct-3B:RFEALQLSFKNMCKLRPLLQKWVEEADNNENLQEICKAETLVQARKRKRTSIENRVRGSLENLFLQCPKPTLQQISHIAQQLGLEKDVVR
                                                                        *
human  Oct-3B:RFEALQLSFKNMCKLRPLLQKWVEEADNNENLQEICKAETLVQARKRKRTSIENRVRGNLENLFLQCPKPTLQQISHIAQQLGLEKDVVR
```

```
monkey Oct-3B:VWFCNRRQKGKRSSSDYAQREDFEAAGSPFSGGPVSFPLAPGPHFGTPGYGSPHFTALYSSVPFPEGEAFPPVPVTTLGSPMHSN
                                                                    *                    *      *
human  Oct-3B:VWFCNRRQKGKRSSSDYAQREDFEAAGSPFSGGPVSFPLAPGPHFGAPGYGSPHFTALYSSVPFPEGEAFPPVSVTTLGSPLHSN
```

C


```
         MEF  CMK6 ——3T3——
          1    2    3    4
Oct-3A
Oct-3B
```

FIG. 1. Predicted amino acid sequences and protein expression of two cynomolgus monkey Oct-3 isoforms. Amino acid sequences of cynomolgus monkey Oct-3A (**A**) and Oct-3B (**B**) were predicted by their nucleic acid sequences. Both monkey Oct-3A and Oct-3B have high homologies to those of humans (98.6% and 98.5%, respectively). Asterisks (*) or dots (.) indicate amino acids that are different between human and monkey, or between human and mouse, respectively. Boxed sequences indicate the motifs in Oct-3, which are proline- and glycine-rich regions, POU-specific, and POU-homeo domains. These three motifs are common in monkey, human, and mouse. Monkey and human Oct-3A is the homolog of mouse Oct-3. Oct-3B does not have a proline- and glycine-rich region, although the POU-specific and POU-homeo domains, and nuclear localization signal (NLS) (gray) at the head of the POU-homeodomain, are common to Oct-3A and Oct-3B. The accession numbers for cynomolgus Oct-3A and Oct-3B in the DNA Data Bank of Japan (DDBJ) are AB243403 and AB243404, respectively. Protein expression of Oct-3 isoforms was examined by Western blotting (**C**). Cynomolgus ES cells (lane 2) expressed Oct-3B (*lower*) as well as Oct-3A (*upper*). Lanes 3 and 4 were Oct-3A and Oct-3B-transfected 3T3 cells used as positive controls: MEF (line 1) was used as a negative control. Oct-3A and Oct-3B were detected using the same anti-Oct-3 antibody whose epitope is common to both isoforms, on the same membrane with different exposure times.

570

FIG. 2. Colony formation of ES cells followed by transfection of Oct-3A and Oct-3B expression vectors in mouse ES cells and cynomolgus ES cells. (A) The surviving colonies of mouse ES cells were detected and their undifferentiated state was examined by ALP staining. (B) The number of total colonies of Oct-3A- and Oct-3B-transfected mouse ES cells was scored as the relative number to that of empty vector (Mock)-transfected cells in each independently repeated experiment. The average scores are presented. (C) The average percentages of undifferentiated (white), partially differentiated (gray), and differentiated (black) colonies in each transfected group are shown. (D) ALP staining of colonies after G418 selection in cynomolgus monkey ES cells is presented. (Scale bar = 500 μm.) (E) Typical appearances of undifferentiated, partially differentiated, and differentiated colonies in monkey ES cells are shown. (F) The total colony number relative to Mock-transfected cynomolgus ES cells was scored and presented. (G) Undifferentiated (white), partially differentiated (gray), and differentiated (black) cynomolgus ES cell colonies were counted. The average percentages are shown. (H) The relative number of total colonies of cynomolgus ES cells transfected with the vectors that were cut between promoter and either Oct-3A or Oct-3B and that did not express exogenous Oct-3A or Oct-3B is shown.
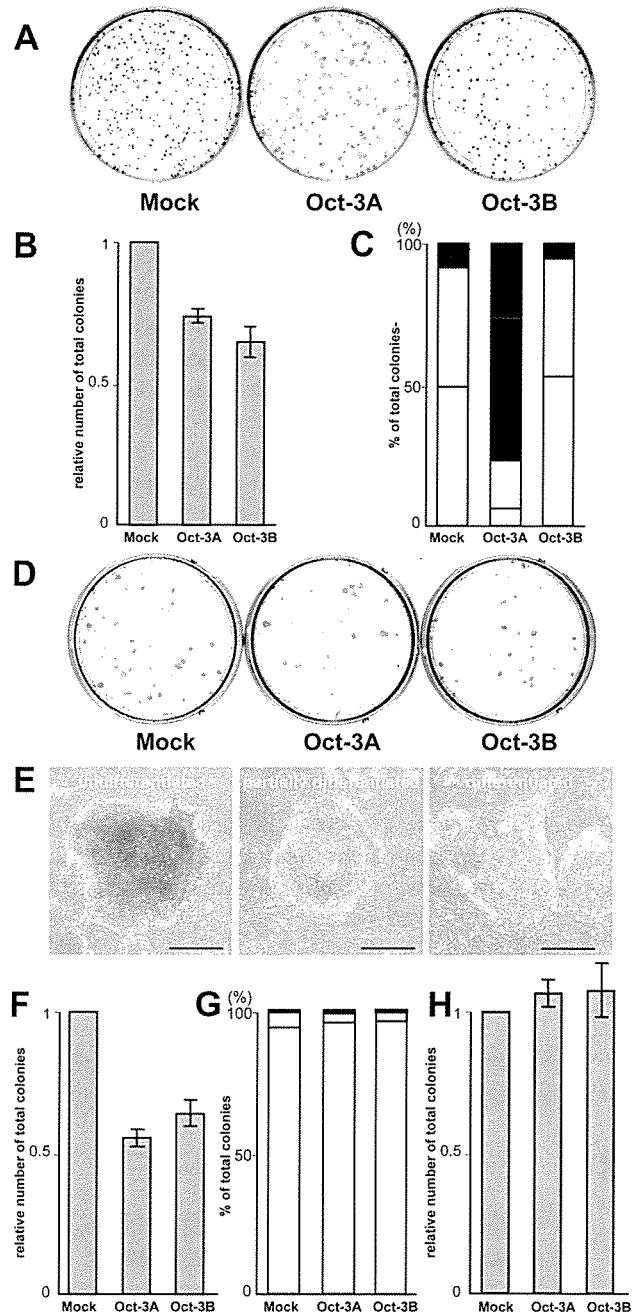
were no differences in the number of colonies among these three groups following transfection of these vectors into cynomolgus ES cells (Fig. 2H). This implied that the reduced number of surviving colonies was due to the effects of exogenous Oct-3A and Oct-3B expression, but not due to differences in the plasmid transfection efficiency. These data suggest that the Oct-3A and Oct-3B up-regulation in monkey ES cells decreased survival or proliferation.

We assumed that the reduced total number of Oct-3A-

and Oct-3B-transfected monkey ES colonies was caused by their differentiation, and that ES cells with high exogenous Oct-3 expression differentiate but do not proliferate. To examine this possibility, we quantified the Oct-3A and Oct-3B protein expression levels in stably transfected cynomolgus ES cell lines.
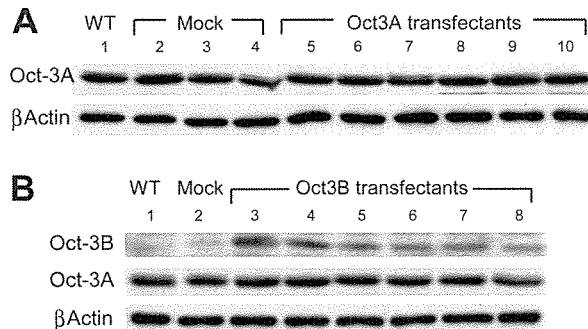
The protein expression level of Oct-3A stable transfectants was not more than 1.5 times that of nontransfected ES cells (wild-type) or mock-transfected cells. We screened the Oct-3A protein expression levels of 18 sta-

571

ble Oct-3A-transfected ES cell lines, but did not find any lines with higher Oct-3A expression. There was no apparent difference in Oct-3A protein levels between Oct-3A and mock-transfected clones (Fig. 3A). These data indicate that only the transfectants with an Oct-3A protein expression level similar to that of wild-type could survive and proliferate. This suggests that the appropriate level of Oct-3A for maintaining self-renewal and proliferation of monkey ES cells is restricted to a certain range, as in the case of Oct-3 in mouse ES cells (19), and that the high-level Oct-3A transfectants in monkey ES cells were probably eliminated during G418 selection.
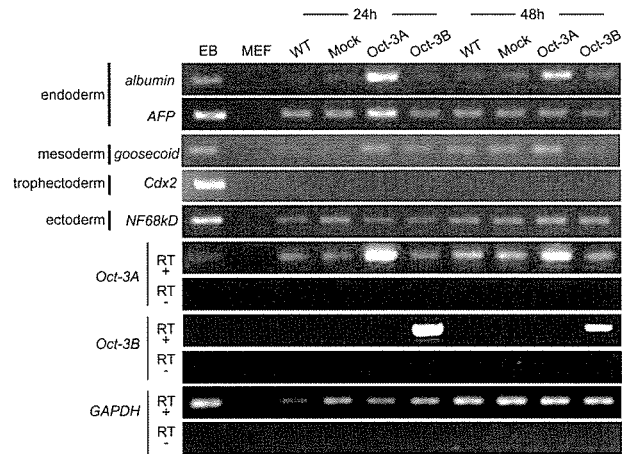
In contrast, among Oct-3B stably transfected ES cell lines, several lines expressed high levels of Oct-3B (Fig. 3B). Of 11 stable Oct-3B transfected ES cell lines, seven clones had more than twice the Oct-3B expression level than the wild type, the highest being 4.9 times the wild-type level. On the other hand, the endogenous Oct-3A expression level was between 0.8 and 1.5 times that of the wild type. No correlation was detected between the expression level of Oct-3B and Oct-3A in any Oct-3B-transfected ES cell line.

Transient expression of Oct-3A promotes differentiation of monkey ES cells

To elucidate whether Oct-3A or Oct-3B overexpression induces differentiation of monkey ES cells, we determined the expression of differentiation marker genes

FIG. 4. Expression of differentiation marker in cynomolgus ES cells transiently transfected with Oct-3A and Oct-3B. Expression of the differentiation markers at 24 and 48 h after transfection of Oct-3A or Oct-3B was examined by RT-PCR. EB was used as a positive control for detecting differentiation markers. MEF was used as a negative control. Neither primer pair crossreacted with mouse cDNA. GAPDH was used as an internal control. RT+ and RT− indicate the presence and absence of reverse transcriptase in the first-strand cDNA reaction, respectively.

FIG. 3. Protein expression levels of Oct-3A or Oct-3B in cynomolgus ES cell lines transfected with Oct-3A and Oct-3B. (A) Oct-3A protein expression level of six different stable Oct-3A-transfected lines (lanes 5–10). Stable Oct-3A transfectants did not have apparently higher levels of Oct-3A expression than wild-type (WT) ES cells (lane 1) or Mock-transfected (lanes 2–4). (B) Oct-3B or Oct-3A protein expression level of six different stable Oct-3B-transfected lines (lanes 3–8). The stable Oct-3B transfectants had up to five-fold higher Oct-3B expression than WT (lane 1) and Mock-transfected cells (lane 2), whereas the Oct-3A expression levels were not different from WT or Mock-transfected cells. β-Actin was used as an internal control.

in monkey ES cells that were transiently transfected with either Oct-3A or Oct-3B vectors by RT-PCR. In the case of transient transfection, *Oct-3A* and *Oct-3B* expression levels peaked 48 h after transfection, and then decreased 72 h after transfection (data not shown). In Oct-3A transfectants, the endoderm markers, *alpha-fetoprotein (AFP)* and *albumin*, and the mesodermal marker, *goosecoid*, had a higher intensity 24 h after transfection than wild-type, mock, or Oct-3B transfectants (Fig. 4). The higher expression level of *albumin* and *goosecoid* in Oct-3A transfectants remained at 48 h after transfection. On the other hand, signal intensities of a trophectoderm marker, *Cdx2*, and an ectoderm marker, *NF68kD*, were not different between wild-type and any of the transfected cells. Differentiation marker expression was not different in Oct-3B-transfected cells compared to those of wild-type and mock-transfected cells. These data suggested that overexpression of Oct-3A, but not Oct-3B, in monkey ES cells promotes differentiation toward endodermal and mesodermal lineages.

DISCUSSION

Oct-3 is a key regulator of early embryonic development and is important for maintaining self-renewal in mouse ES cells (18,19). In humans, there are two Oct-3 isoforms, Oct-3A and Oct-3B (25). Oct-3A is a homolog of mouse Oct-3, and they share 87% amino acid identity

572

(25). Oct-3B is a splicing variant of Oct-3A (25). In mouse, there is no isoform such as Oct-3B (25). There are no previous reports on the expression of Oct-3 isoforms or their functions in primate ES cells. In our study, we confirmed mRNA and protein expression of Oct-3 isoforms, Oct-3A and Oct-3B, in cynomolgus monkey ES cells, and determined that their sequences had high homology to the human Oct-3 isoforms.

The present study examined the effects of Oct-3A and Oct-3B overexpression on primate ES cells. The total number of surviving stable Oct-3A-transfected colonies was reduced to approximately 55% that of mock-transfected cells, and most of the surviving colonies remained in an undifferentiated state. Among the stably transfected monkey ES cell lines, none of the cell lines expressed high levels of Oct-3A. In the transient transfection assay, overexpression of Oct-3A in monkey ES cells induced an increase in endoderm and mesoderm markers. These data suggest that high Oct-3A expression promoted ES cell differentiation, and, therefore, cells with high Oct-3A expression do not proliferate or survive. In mouse ES cells, most of the surviving colonies were differentiated. It is possible that both mouse and monkey ES cells were differentiated due to Oct-3A overexpression, although the ratio of differentiated colonies were different between them. This might have been due to differences in viability of differentiated cells of each species. Alternatively, the Oct-3A-transfected primate ES cells might stop proliferation immediately after differentiation, whereas the Oct-3A transfected mouse ES cells might continue proliferation even after differentiation for a certain period.

We confirmed that Oct-3B is expressed in monkey ES cells at low but detectable levels. As in the case of Oct-3A, the total number of stable Oct-3B transfectants was reduced, and the ratio of undifferentiated colonies was not different from those of mock-transfected cells. Transient transfection of Oct-3B and RT-PCR analysis in monkey ES cells, however, failed to demonstrate any increase in the differentiation markers. Unlike Oct-3A transfection, several cell lines of stable Oct-3B transfectants had higher Oct-3B expression than wild-type ES cells. Therefore, Oct-3B overexpression might have had some influence on the viability of monkey ES cells, although it does not appear to have induced the differentiation of monkey ES cells. Stable Oct-3B-transfected monkey ES cell lines had up to five-fold higher Oct-3B expression than wild type. The amount of Oct-3B protein, however, was much smaller than that of Oct-3A, even in cells with the highest level of Oct-3B expression. Thus, Oct-3B overexpression might have little impact on the proliferation of monkey ES cells.

In summary, this is the first report of two Oct-3 isoforms, Oct-3A and Oct-3B, expressed in monkey ES cells. The overexpression of Oct-3A, but not Oct-3B, promoted differentiation of monkey ES cells into endoder-

mal and mesodermal lineages. It is likely that there is a mechanism similar to that reported in mouse ES cells (19) to regulate the level of Oct-3A for maintaining self-renewal of primate ES cells. For further studies on the proper range of Oct-3A expression and the function of Oct-3B in primate ES cells, regulatable gene expression systems enable the control of Oct-3A and Oct-3B levels, including endogenous expression. Possible approaches include the combination of gene targeting of wild-type *POU5F1* alleles and an inducible system to control exogenous expression of Oct-3A or Oct-3B in primate ES cells.

REFERENCES

1. Evans MJ and MH Kaufman. (1981). Establishment in culture of pluripotential cells from mouse embryos. Nature 292:154–156.
2. Bradley A, M Evans, MH Kaufman and E Robertson. (1984). Formation of germ-line chimaeras from embryo-derived teratocarcinoma cell lines. Nature 309:255–256.
3. Thomson JA, J Kalishman, TG Golos, M Durning, CP Harris, RA Becker and JP Hearn. (1995). Isolation of a primate embryonic stem cell line. Proc Natl Acad Sci USA 92:7844–7848.
4. Thomson JA, J Kalishman, TG Golos, M Durning, CP Harris and JP Hearn. (1996). Pluripotent cell lines derived from common marmoset (*Callithrix jacchus*) blastocysts. Biol Reprod 55:254–259.
5. Suemori H, T Tada, R Torii, Y Hosoi, K Kobayashi, H Imahie, Y Kondo, A Iritani and N Nakatsuji. (2001). Establishment of embryonic stem cell lines from cynomolgus monkey blastocysts produced by IVF or ICSI. Dev Dyn 222:273–279.
6. Thomson JA, J Itskovitz-Eldor, SS Shapiro, MA Waknitz, JJ Swiergiel, VS Marshall and JM Jones. (1998). Embryonic stem cell lines derived from human blastocysts. Science 282:1145–1147.
7. Takagi Y, J Takahashi, H Saiki, A Morizane, T Hayashi, Y Kishi, H Fukuda, Y Okamoto, M Koyanagi, M Ideguchi, H Hayashi, T Imazato, H Kawasaki, H Suemori, S Omachi, H Iida, N Itoh, N Nakatsuji, Y Sasai and N Hashimoto. (2005). Dopaminergic neurons generated from monkey embryonic stem cells function in a Parkinson primate model. J Clin Invest 115:102–109.
8. Boeuf H, C Hauss, FD Graeve, N Baran and C Kedinger. (1997). Leukemia inhibitory factor-dependent transcriptional activation in embryonic stem cells. J Cell Biol 138:1207–1217.

573

195

9. Matsuda T, T Nakamura, K Nakao, T Arai, M Katsuki, T Heike and T Yokota. (1999). STAT3 activation is sufficient to maintain an undifferentiated state of mouse embryonic stem cells. EMBO J 18:4261–4269.

10. Sumi T, Y Fujimoto, N Nakatsuji and H Suemori. (2004). STAT3 is dispensable for maintenance of self-renewal in nonhuman primate embryonic stem cells. Stem Cells 22:861–872.

11. Beattie GM, AD Lopez, N Bucay, A Hinton, MT Firpo, CC King and A Hayek. (2005). Activin A maintains pluripotency of human embryonic stem cells in the absence of feeder layers. Stem Cells 23:489–495.

12. Xu RH, X Chen, DS Li, R Li, GC Addicks, C Glennon, TP Zwaka and JA Thomson. (2002). BMP4 initiates human embryonic stem cell differentiation to trophoblast. Nature Biotechnol 20:1261–1264.

13. Ying QL, J Nichols, I Chambers and A Smith. (2003). BMP induction of Id proteins suppresses differentiation and sustains embryonic stem cell self-renewal in collaboration with STAT3. Cell 115:281–292.

14. Qi X, TG Li, J Hao, J Hu, J Wang, H Simmons, S Miura, Y Mishina and GQ Zhao. (2004). BMP4 supports self-renewal of embryonic stem cells by inhibiting mitogen-activated protein kinase pathways. Proc Natl Acad Sci USA 101:6027–6032.

15. Okamoto K, H Okazawa, A Okuda, M Sakai, M Muramatsu and H Hamada. (1990). A novel octamer binding transcription factor is differentially expressed in mouse embryonic cells. Cell 60:461–472.

16. Scholer HR, S Ruppert, N Suzuki, K Chowdhury and P Gruss. (1990). New type of POU domain in germ line-specific protein Oct-4. Nature 344:435–439.

17. Rosner MH, MA Vigano, K Ozato, PM Timmons, F Poirier, PW Rigby and LM Staudt. (1990). A POU-domain transcription factor in early stem cells and germ cells of the mammalian embryo. Nature 345:686–692.

18. Nichols J, B Zevnik, K Anastassiadis, H Niwa, D Klewe-Nebenius, I Chambers, H Scholer and A Smith. (1998). Formation of pluripotent stem cells in the mammalian embryo depends on the POU transcription factor Oct4. Cell 95:379–391.

19. Niwa H, J Miyazaki and AG Smith. (2000). Quantitative expression of Oct-3/4 defines differentiation, dedifferentiation or self-renewal of ES cells. Nature Genet 24:372–376.

20. Scholer HR, AK Hatzopoulos, R Balling, N Suzuki and P Gruss. (1989). A family of octamer-specific proteins present during mouse embryogenesis: evidence for germline-specific expression of an Oct factor. EMBO J 8:2543–2550.

21. Lenardo MJ, L Staudt, P Robbins, A Kuang, RC Mulligan and D Baltimore. (1989). Repression of the IgH enhancer in teratocarcinoma cells associated with a novel octamer factor. Science 243:544–546.

22. Scholer HR, GR Dressler, R Balling, H Rohdewohld and P Gruss. (1990). Oct-4: a germline-specific transcription factor mapping to the mouse t-complex. EMBO J 9:2185–2195.

23. Palmieri SL, W Peter, H Hess and HR Scholer. (1994). Oct-4 transcription factor is differentially expressed in the mouse embryo during establishment of the first two extraembryonic cell lineages involved in implantation. Dev Biol 166:259–267.

24. Yeom YI, G Fuhrmann, CE Ovitt, A Brehm, K Ohbo, M Gross, K Hubner and HR Scholer. (1996). Germline regulatory element of Oct-4 specific for the totipotent cycle of embryonal cells. Development 122:881–894.

25. Takeda J, S Seino and GI Bell. (1992). Human Oct3 gene family: cDNA sequences, alternative splicing, gene organization, chromosomal location, and expression at low levels in adult tissues. Nucleic Acids Res 20:4613–4620.

26. Niwa H, S Masui, I Chambers, AG Smith and J Miyazaki. (2002). Phenotypic complementation establishes requirements for specific POU domain and generic transactivation function of Oct-3/4 in embryonic stem cells. Mol Cell Biol 22:1526–1536.

27. Smith AE and KG Ford. (2005). Use of altered-specificity binding Oct-4 suggests an absence of pluripotent cell-specific cofactor usage. Nucleic Acids Res 33:6011–6023.

28. Cauffman G, H Van de Velde, I Liebaers and A Van Steirteghem. (2005). Oct-4 mRNA and protein expression during human preimplantation development. Mol Hum Reprod 11:173–181.

29. Hay DC, L Sutherland, J Clark and T Burdon. (2004). Oct-4 knockdown induces similar patterns of endoderm and trophoblast differentiation markers in human and mouse embryonic stem cells. Stem Cells 22:225–235.

30. Matin MM, JR Walsh, PJ Gokhale, JS Draper, AR Bahrami, I Morton, HD Moore and PW Andrews. (2004). Specific knockdown of Oct4 and beta2–microglobulin expression by RNA interference in human embryonic stem cells and embryonic carcinoma cells. Stem Cells 22:659–668.

31. Nagy A, J Rossant, R Nagy, W Abramow-Newerly and JC Roder. (1993). Derivation of completely cell culture-derived mice from early-passage embryonic stem cells. Proc Natl Acad Sci USA 90:8424–8428.

32. Niwa H, K Yamamura and J Miyazaki. (1991). Efficient selection for high-expression transfectants with a novel eukaryotic vector. Gene 108:193–199.

Address reprint requests to:
Dr. Hirofumi Suemori
Laboratory of Embryonic Stem Cell Research
Stem Cell Research Center
Institute for Frontier Medical Sciences
Kyoto University
53 Kawahara-cho, Shogoin, Sakyo-ku
Kyoto, 606-8507, Japan

E-mail: hsuemori@frontier.kyoto-u.ac.jp

Non-organic hearing loss

HARUKAZU HIRAUMI[1], JUN TSUJI[2], SHIN-ICHI KANEMARU[1], KIYOHIRO FUJINO[1] & JUICHI ITO[1]

[1]*Department of Otolaryngology-Head & Neck Surgery, Graduate School of Medicine, Kyoto University and* [2]*Department of Otolaryngology-Bronchoesophagology, Kyoto Medical Center, Kyoto, Japan*

Abstract
Conclusion. Most non-organic hearing loss (NOHL) patients were young females. The discrepancy between the results of pure tone audiometry and objective auditory testing suggests NOHL. The diagnostic problem is that objective audiometry is not included in routine examinations and we have to suspect NOHL in order to perform further examination. The correct diagnosis can be difficult in patients who present with unilateral sudden hearing loss or who also have moderate to profound organic hearing loss. *Objective.* Symptoms and results of auditory tests for NOHL patients were reviewed. *Patients and methods.* This study comprised 31 patients with NOHL. Age, symptoms, and the results of subjective and objective audiometry were collected. *Results.* Twenty-four patients were female and 7 were male. The age at attendance ranged from 7 to 39 years old, with an average age of 16.6 years. Eight patients received steroids before the correct diagnosis was made. Six of them presented with unilateral sudden hearing loss, and the other two patients had accompanying bilateral organic hearing loss.

Keywords: *Non-organic hearing loss, diagnosis, sudden hearing loss*

Introduction

Non-organic hearing loss (NOHL) is a condition in which there is a discrepancy between the actual hearing threshold and admitted threshold of the patients. Various terms are used to describe this condition, including functional hearing loss, pseudohypacusis, psychogenic hearing loss, and conversion deafness. Some authors use these terms to describe different conditions [1], but the differences are obscure. The term NOHL is the most neutral one, and we use it in this paper. NOHL is a well-known clinical entity, but is often forgotten in the daily clinical setting. In most cases, the diagnosis of NOHL is easy, but in some cases the correct diagnosis is difficult and inappropriate treatments including steroid administration can be administered. Such diagnostic difficulty has not been mentioned in previous reports. In this manuscript, we review the etiology and the symptoms of NOHL patients and clarify the problems in the diagnosis of NOHL.

Patients and methods

Thirty-one NOHL patients attended the Kyoto University Hospital Department of Otolaryngology-Head and Neck Surgery between April 1, 2000 and March 31, 2005. All patients underwent pure tone audiometry with AA-98 or AA-72 (RION). The diagnosis of NOHL is made when at least one of the following two characteristics is observed: (1) discrepancy between subjective and objective hearing evaluation test, and/or (2) clinically unexplainable audiological symptoms including prominent fluctuations of the threshold in the pure tone audiometry and lower threshold in speech audiometry than the threshold in the pure tone audiometry. Objective hearing thresholds are obtained using distortion product otoacoustic emissions (DPOAEs; CUBeDIS II, Mimosa Acoustics) and/or auditory evoked brainstem response (ABR; MEB-2200, Nihon Kohden). Speech audiometry was performed using the 67-S word lists for Japanese.

Correspondence: H. Hiraumi, Department of Otolaryngology-Head and Neck Surgery, Graduate School of Medicine, Kyoto University, 54 Shogoin-Kawaharacho, Sakyo-ku, Kyoto 606-8507, Japan. Tel: +81 75 751 3346. Fax: +81 75 751 7225. E-mail: hhiraumi@ent.kuhp.kyoto-u.ac.jp
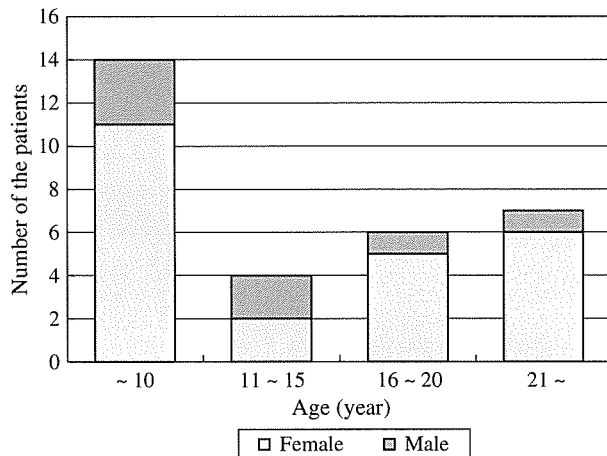
Figure 1. Number of patients according to their ages. Age at attendance ranged from 7 to 39 years old. Twenty-four patients were female and 7 were male. Most of the patients were young females.

Results

Twenty-four patients were female and 7 were male. The age at attendance ranged from 7 to 39 years old, with an average age of 16.6 years (Figure 1). Fifteen patients presented with sudden deterioration of hearing and/or tinnitus. Nine patients complained of progressive hearing loss. The other seven patients had no accompanying subjective symptoms and hearing loss was detected in the school screening hearing test or follow-up study for the organic hearing loss. Fourteen patients presented with unilateral hearing loss. Fourteen patients showed bilateral hearing loss. The other three patients had profound organic hearing loss in one ear and NOHL in the other ear. Among 14 unilateral NOHL patients, 8 patients developed contralateral NOHL afterwards. A total of 53 ears were diagnosed as NOHL.

The average pure tone audiometry threshold ranged from 16.7 dBHL to scale-out (Figure 2). The patterns of the pure tone audiograms were as follows: flat pattern in 33 ears, deaf pattern in 11 ears, hearing loss in both low and high frequencies in 5 ears, dip pattern in 2 ears, and hearing loss at high frequencies in 2 ears. Nine patients also had organic hearing loss: otitis media with effusion (three patients); large vestibular aquaduct syndrome (one); otosclerosis (one); endolymph hydrops (one); contralateral acoustic neurinoma (one); old idiopathic sudden sensorineural hearing loss (ISSNHL; one); and progressive sensorineural hearing loss (one). Seventeen patients were tested by DPOAEs, and 24 patients were tested by ABR. Thirteen patients underwent both DPOAEs and
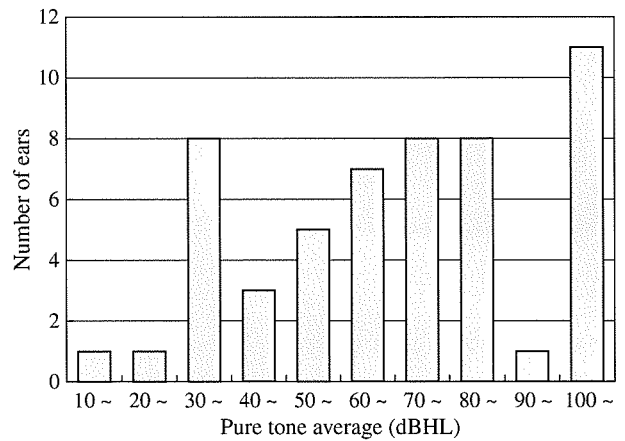

Figure 2. Number of ears according to their thresholds. The threshold distribution was trimodal, with a first peak at 30 dBHL, second peak at 70–80 dBHL, and third peak at >100 dBHL.

ABR testing. In total, 28 patients underwent an objective hearing test. In two patients DOPAEs failed to reveal NOHL because of inappropriate ear-piece insertion. In two patients, ABR was not able to reveal NOHL because of underlying organic hearing loss at high frequencies. Speech audiometry was performed in six patients. Four patients showed >90% speech discrimination at lower level than the threshold in the pure tone audiometry.

Twenty-four patients consulted other doctors first and were referred to our hospital, and 13 of them had received some kind of treatment. Seven patients were admitted to Kyoto University Hospital directly, and one of them was administered high-dose steroid therapy with the diagnosis of organic hearing loss. In total, 14 patients received inappropriate treatment before the diagnosis of NOHL, 8 of whom received steroids. In six of them, hearing loss emerged as unilateral sudden hearing loss, and the other two patients had accompanying bilateral organic hearing loss.

Three representative cases are described below.

Case 1

A 33-year-old man presented with sudden progress of right tinnitus 4 days previously. The pure tone audiogram showed moderate to profound sensorineural hearing loss at all frequencies (Figure 3). He had contracted right ISSNHL 2 years earlier and received high-dose steroid therapy, leaving hearing loss between 250 Hz and 1000 Hz. Prior ISSNHL had been confirmed with DPOAEs, and recurrent hearing loss was suspected at first. However, the patient was very nervous about the deterioration of hearing, and he was tested with ABR. The ABR